

Accepted Manuscript

Formononetin-induced oxidative stress abrogates the activation of STAT3/5 signaling axis and suppresses the tumor growth in multiple myeloma preclinical model

Chulwon Kim, Seok-Geun Lee, Woong Mo Yang, Frank Arfuso, Jae-Young Um, Alan Prem Kumar, Jinsong Bian, Gautam Sethi, Kwang Seok Ahn



PII: S0304-3835(18)30371-9

DOI: [10.1016/j.canlet.2018.05.038](https://doi.org/10.1016/j.canlet.2018.05.038)

Reference: CAN 13922

To appear in: *Cancer Letters*

Received Date: 2 December 2017

Revised Date: 23 May 2018

Accepted Date: 23 May 2018

Please cite this article as: C. Kim, S.-G. Lee, W.M. Yang, F. Arfuso, J.-Y. Um, A.P. Kumar, J. Bian, G. Sethi, K.S. Ahn, Formononetin-induced oxidative stress abrogates the activation of STAT3/5 signaling axis and suppresses the tumor growth in multiple myeloma preclinical model, *Cancer Letters* (2018), doi: 10.1016/j.canlet.2018.05.038.

This is a PDF file of an unedited manuscript that has been accepted for publication. As a service to our customers we are providing this early version of the manuscript. The manuscript will undergo copyediting, typesetting, and review of the resulting proof before it is published in its final form. Please note that during the production process errors may be discovered which could affect the content, and all legal disclaimers that apply to the journal pertain.

Formononetin-induced oxidative stress abrogates the activation of STAT3/5 signaling axis and suppresses the tumor growth in multiple myeloma preclinical model

Chulwon Kim^a, Seok-Geun Lee^a, Woong Mo Yang^a, Frank Arfuso^b, Jae-Young Um^a, Alan Prem Kumar^c, Jinsong Bian^c, Gautam Sethi^{c*}, and Kwang Seok Ahn^{a,*}

^aCollege of Korean Medicine, Kyung Hee University, 24 Kyungheedaero, Dongdaemun-gu, Seoul 02447, Republic of Korea

^bStem Cell and Cancer Biology Laboratory, School of Biomedical Sciences, Curtin Health Innovation Research Institute, Curtin University, Perth WA, 6009 Australia

^cDepartment of Pharmacology, Yong Loo Lin School of Medicine, National University of Singapore, Singapore 117600, Singapore

Running Title: Formononetin exerts anticancer effects in multiple myeloma

Address correspondence to:

Dr. Kwang Seok Ahn, Department of Korean Pathology, College of Korean Medicine, Kyung Hee University, 1 Hoegi-Dong Dongdaemun-Gu, Seoul 130-701, Republic of Korea. Phone: 82-2-961-2316; Email: ksahn@khu.ac.kr

Dr. Gautam Sethi, Department of Pharmacology, National University of Singapore, Singapore, 129800, Email phcgs@nus.edu.sg

Abstract

Aberrant reactions of signal transducer and transcriptional activator (STAT) are frequently detected in multiple myeloma (MM) cancers and can upregulate the expression of multiple genes related to cell proliferation, survival, metastasis, and angiogenesis. Therefore, agents capable of inhibiting STAT activation can form the basis of novel therapies for MM patients. In the present study, we investigated whether the potential anti-cancer effects of Formononetin (FT), a naturally occurring isoflavone derived from *Astragalus membranaceus*, *Trifolium pratense*, *Glycyrrhiza glabra*, and *Pueraria lobata*, against MM cell lines and human multiple myeloma xenograft tumors in athymic nu/nu mice model are mediated through the negative regulation of STAT3 and STAT5 pathways. Data from the *in vitro* studies indicated that FT could significantly inhibit cell viability, and induce apoptosis. Interestingly, FT also suppressed constitutive STAT3 (tyrosine residue 705 and serine residue 727) and STAT5 (tyrosine residue 694/699) activation, which correlated with the suppression of the upstream kinases (JAK1, JAK2, and c-Src) in MM cells, and this effect was found to be mediated *via* an increased production of reactive oxygen species (ROS) due to GSH/GSSG imbalance. Also, FT abrogated STAT3 and STAT5 DNA binding capacity and nuclear translocation. FT induced cell cycle arrest, downregulated the expression of STAT3-regulated anti-apoptotic, angiogenic, and proliferative gene products; and this correlated with induction of caspase-3 activation and cleavage of PARP. Intraperitoneal administration of FT significantly suppressed the tumor growth in the multiple myeloma xenograft mouse model without exhibiting any significant adverse effects. Overall, our findings indicate that FT exhibits significant anti-cancer effects in MM that may be primarily mediated through the ROS-regulated inhibition of the STAT3 and STAT5 signaling cascade.

Keywords: Formononetin; STAT; ROS; multiple myeloma

1. Introduction

Multiple myeloma (MM) is a malignant B-cell neoplasm that is characterized by the accumulation of malignant plasma cells in the bone marrow, accounting for about 10% of all hematologic malignancies [1-5]. The clonal B cell neoplasm proceeds through different phases: an inactive phase in which tumor cells are non-proliferating mature plasma cells; an active phase with a small proportion (1%) of proliferating plasmablastic cells; and a fulminant phase with the frequent occurrence of extramedullary proliferation and an increase in plasmablastic cells [6]. Homing and expansion of the malignant plasma cells to occupy the bone marrow niche, monoclonal protein production, anemia, osteolytic bone lesions, renal failure, and immunodeficiency are major clinical features of MM patients [7-9]. Despite the introduction of several new treatment protocols, including proteasome inhibitors, immunomodulatory agents, corticosteroids, and alkylating agents, for the treatment of MM patients who have recently been diagnosed, MM remains an incurable and fatal disease [10-12].

Signal transducer and activator of transcription (STAT) proteins, firstly discovered as latent cytoplasmic transcription factors about two decades ago [13-16], consist of seven diverse members, STAT1 to STAT6, STAT5a, and STAT5b [17], which have been found to play a critical role in both inflammation and tumorigenesis [18]. Among the different STATs, STAT3 and STAT5 are often constitutively active in various human cancers, such as multiple myeloma (MM), leukemia, lymphoma, hepatocellular carcinoma (HCC), breast cancer, prostate cancer, renal cell carcinoma (RCC), head and neck squamous cell carcinoma, and several other malignancies [19-24], and control the expression of multiple genes involved in cancer initiation, progression, and chemoresistance [23, 25-30]. Normally, STAT3 is present in an inactive form as a monomer in the cytoplasm; once the STAT monomer is phosphorylated by the receptor-associated tyrosine kinases, Janus activated kinases (JAK), JAK1, JAK2, JAK3, and TYK2 [13, 20, 31-33], it can induce active dimers and then migrate into the nucleus to undergo DNA binding and subsequent gene transcription [18, 33, 34]. STAT3 and STAT5 has been found to regulate the expression of a plethora of genes involved in anti-apoptosis, proliferation, and angiogenesis in MM [35-38]. Thus, identification of novel pharmacological agents that inhibit STAT3 and STAT5 activation has promise and potential in the prevention and therapy of cancer [39].

Currently, several strategies have been reported to block the action of the kinase signaling pathway, including natural compounds, peptidomimetic compounds, and small molecules. The discovery of novel anti-cancer agents derived from existing natural sources provides an enormous opportunity to enhance the existing standard of care for various human cancers [40-45]. Formononetin (7-hydroxy-3-(4-methoxyphenyl) chromen-4-one) is a naturally occurring isoflavone, which can be found in the roots of *Astragalus membranaceus*, *Trifolium pratense*, *Glycyrrhiza glabra*, and *Pueraria lobata*. Preclinical studies demonstrate that FT is associated with inhibition of cancer cell proliferation, and can induce apoptosis in diverse cancers such as prostate, bladder, breast, cervical, lung, colorectal, nasopharyngeal, and leukemia [46-55]. Furthermore, it possesses anti-angiogenic activity in human colon cancer cells and tumor xenograft [56]. Interestingly, low concentration of FT has been reported to stimulate the proliferation of nasopharyngeal carcinoma cell line by upregulating Bcl-2 and p-ERK1/2 expression [57], and it has also been found to exert pro-angiogenesis effects through an ER α -enhanced ROCK-II signaling pathways [58]. However, data on the influence of FT on MM cells and the underlying mechanisms are yet to be fully elucidated.

Hence, the discovery of novel therapeutics or molecular targeting therapies for multiple MM remains a priority. Targeting apoptotic pathways appears as a promising approach to prevent and treat cancers. Previous reports show a high frequency of increased STAT activation in MM cells [21, 30, 59]. Because of the pivotal role of STATs in tumor cell survival, proliferation, and angiogenesis, we hypothesized that STATs could be a novel therapeutic target for MM. Thus, in our study, we examined whether FT can mediate its anti-cancer effects in part through the abrogation of the STAT activation pathway.

2. Materials and methods

2.1.1 Reagents

Formononetin (FT) was purchased from Selleck Chemicals (Houston, TX). 3-(4,5-dimethylthiazol-2-yl)-2,5-diphenyltetrazolium bromide (MTT), propidium iodide (PI), Tris base, glycine, NaCl, sodium dodecylsulfate (SDS), bovine serum albumin (BSA), N-acetyl-L-cysteine (NAC), glutathione (GSH), and buthionine sulfoximine (BSO) were purchased from Sigma-Aldrich (St. Louis, MO). RPMI 1640, fetal bovine serum (FBS), antibiotic-antimycotic mixture, and LightShift[®] Chemiluminescent EMSA kit, cell-permeant 2',7'-dichlorodihydrofluorescein diacetate (H₂DCF-DA) were obtained from Thermo Fisher Scientific Inc. (Waltham, MA). 5'-biotinylated STAT3 and STAT5 were obtained from Bioneer Corporation (Daejeon, Korea). Alexa Fluor[®] 488 donkey anti-goat IgG (H+L) antibody, Alexa Fluor[®] 594 donkey anti-rabbit IgG (H+L) antibody, and 0.4% trypan blue vital stain were obtained from Life Technologies (Grand Island, NY). IL-6 was obtained from R&D Systems (Minneapolis, MN). Anti-phospho-STAT3(Tyr705), anti-phospho-STAT3(Ser727), anti-phospho-JAK1(Tyr1022/1023), anti-JAK1, anti-phospho-JAK2(Tyr1007/1008), anti-JAK2, anti-phospho-Src(Tyr416), anti-Flag, anti-cleaved caspase-3, anti-CDK2, anti-CDK4, anti-Cyclin E, anti-Cyclin D1, and anti-glutathione reductase (GR) antibodies were purchased from Cell Signaling Technology (Beverly, MA). Anti-STAT3, anti-phospho-STAT5(Tyr 694/Tyr 699), anti-STAT5, anti-Src, anti-Bcl-2, anti-Survivin, anti-IAP-2, anti-VEGF, anti-Cyclin B1, anti-Ki-67, anti-CD31, anti-caspase-3, anti-PARP, anti- β -actin, and horseradish peroxidase (HRP)-conjugated secondary antibodies were obtained from Santa Cruz Biotechnology (Santa Cruz, CA). Anti-GSH antibodies were obtained from Abcam (Cambridge, MA). Bortezomib (Bor) was obtained from LC Laboratories (Woburn, MA). STAT3-C Flag pRc/CMV were obtained from Addgene (Cambridge, MA).

2.1.2 Cell lines

Human multiple myeloma cell line U266 and human myeloma cell line RPMI 8226 were obtained from the American Type Culture Collection (Manassas, VA). U266 and RPMI 8226 cells were cultured in RPMI 1640 medium containing 10% FBS. Media were also supplemented with 100 U/ml of penicillin and 100 μ g/ml of streptomycin.

2.1.3 Isolation of human peripheral blood mononuclear cells (PBMC)

Human peripheral blood mononuclear cells (PBMC) were isolated from the blood of healthy adult volunteer donors by density gradient centrifugation on Lymphoprep (Axis-Shield PoC AS, Oslo, Norway).

2.1.4 Western blotting

After the cells were treated with the indicated concentrations of FT, the cells were lysed and the total protein concentrations were determined by Bradford reagent (Bio-Rad, Hercules, CA). Equal amounts of lysates resolved on sodium dodecyl-polyacrylamide gel electrophoresis (SDS-PAGE) were transferred to a nitrocellulose membrane, and the membrane was blocked with 1 \times TBS containing 0.1% Tween 20 and 5% skim milk or 2% BSA for 1 h at room temperature. After the blocking, the membranes were incubated overnight at 4 $^{\circ}$ C with the respective primary antibodies. The membranes were washed twice and incubated with diluted horseradish peroxidase (HRP)-conjugated secondary antibodies (1:10000) for 1 h at room temperature. After three washes, the membranes were detected using an enhanced chemiluminescence (ECL) kit (Millipore, Bedford, MA).

2.1.5 EMSA for STAT3 and STAT5-DNA binding

STAT3 and STAT5-DNA binding was analyzed by an electrophoretic mobility shift assay (EMSA) using a 5'-biotinylated STAT3 oligonucleotide (5'-GATCCTTCTGGGAATTCCTAGATC-3' and 5'-GATCTAGGAATTCCTAGGAAGGATC-3') and 5'-biotinylated STAT5 oligonucleotide (5'-AGA TTT CTA GGA ATT CAA TCC-3' and 5'-GGA TTG AAT TCC TAG AAA TCT-3'). Briefly, nuclear extracts were prepared from FT treated cells and incubated with the 5'-biotinylated STAT3 and STAT5 oligonucleotide probes. The DNA-protein complex formed was separated from free oligonucleotide on 6% native polyacrylamide gels and transferred to a positively charged nylon membrane. The membrane was detected following the manufacturer's instructions using LightShift[®] Chemiluminescent EMSA kit (Waltham, MA).

2.1.6 Immunocytochemistry for STAT3 and STAT5 localization

After the U266 cells were treated with 100 μ M of FT, the cell suspension was put into a cytospin and the assembly was placed into the rotor. Thereafter it was centrifuged for 5 min at 750 rpm. The cells were attached to the slide and analyzed under a microscope to determine if a monolayer spread of cells was obtained. The cells were fixed in 4% paraformaldehyde (PFA) for 20 min at room temperature and then washed three times in PBS. The cells were permeabilized with 0.2% Triton X-100 in PBS for 20 min, washed three times in PBS, and then blocked with 5% bovine serum albumin in PBS for 1 h at room temperature. The cells were then incubated overnight at 4 $^{\circ}$ C with anti-phospho-STAT3(Tyr705) (1:100; Cell Signaling Technology), anti-STAT3, anti-phospho-STAT5(Tyr 694/Tyr 699), and anti-STAT5 (1:100; Santa Cruz), washed three times, and then incubated with Alexa Fluor[®] 488 donkey anti-goat IgG (H+L) antibody and Alexa Fluor[®] 594 donkey anti-rabbit IgG (H+L) antibody for 1 h at room temperature. Next, the cells were stained with 1 μ g/ml DAPI solution and mounted on glass slides using Fluorescent Mounting Medium (Golden Bridge International Labs, Mukilteo, WA). Using an Olympus FluoView FV1000 confocal microscope (Tokyo, Japan), DAPI and FITC fluorescence were excited (Ex: 405 nm and 488 nm) and detected (Em: 461 nm and 519 nm) with 2.1% laser transmissivity and 5.0% laser transmissivity, respectively.

2.1.7 STAT3 luciferase reporter assay

The cells were transfected using the Neon[™] Transfection System (Invitrogen, Carlsbad, CA). Transfection efficiency was measured by Western blot analysis. RPMI 8226 cells were prepared for transfection after the cells were resuspended with 120 μ l of Neon Resuspension Buffer R for every one million cells. The STAT3-responsive elements linked to a luciferase reporter gene were transfected with wildtype or dominant-negative STAT3-Y705F (STAT3F). These plasmids were aliquoted into a sterile

microcentrifuge tube. A Neon Tip was inserted into the Neon Pipette and the cell-plasmids mixture was aspirated into the tip, avoiding air bubbles. The Neon Pipette was then inserted into the Neon Tube containing 3 ml of Neon Electrolytic Buffer E in the Neon Pipette Station. Cells were pulsed once with a voltage of 1,200 and a width of 20 ms. After 48 h of transfection, cells were treated with 50, 75, and 100 μ M of FT for 6 h and then stimulated with IL-6 (10 ng/mL) for 15 min. Whole-cell extracts were then prepared and analyzed for luciferase activity.

2.1.8 Transfection of plasmids

U266 cells were prepared for transfection after cells were resuspended with 120 μ l of Neon Resuspension Buffer R for every one million cells. For each electroporation, U266 cells with 1 μ g of STAT3-C Flag pRc/CMV or empty vector plasmids were aliquoted into a sterile microcentrifuge tube. A Neon Tip was inserted into the Neon Pipette and the mixture was aspirated into the tip avoiding air bubbles. The Neon Pipette was then inserted into the Neon Tube containing 3 ml of Neon Electrolytic Buffer E in the Neon Pipette Station. U266 cells were pulsed twice with a voltage of 1,150 and a width of 30. After 48 h of transfection, cells were seeded for Western blotting and MTT assay.

2.1.9 Reverse Transcription Polymerase Chain Reaction (RT-PCR)

Cells were washed and suspended in Trizol reagent. Total RNA was extracted according to the manufacturer's instructions (Invitrogen, Life Technologies, Carlsbad, CA). One microgram of total RNA was converted to cDNA by superscript reverse transcriptase and then amplified by a Taq polymerase using reverse transcription polymerase chain reaction (RT-PCR) (TAKARA, Tokyo, Japan). The relative expressions of *BCL-2* and *Survivin* were analyzed using PCR with glyceraldehyde-3-phosphate dehydrogenase (GAPDH) as an internal control. The following pairs of forward and reverse primer sets were used: *BCL-2*, 5'-TTGTGGCCTTCTTTGAGTTCGGTG-3' and 5'-TACAGTTCACAAAGGCATCCCAG-3'. *Survivin*, 5'-ATGGGTGCCCGACGTT-3' and 5'-TCAATCCATGGCAGCCAG-3'. The cDNA reaction was performed at 45°C for 60 min and 95°C for 5 min. PCR products were run on 1% agarose gel and then stained with Loading Star (Dynebio, Seongnam, Korea). Stained bands were visualized under UV light and photographed.

2.2 Cell cycle analysis

To determine apoptosis, cell cycle analysis was performed using PI. After treatment with 100 μ M of FT, the cells were collected, washed with cold PBS, fixed with 70% ethanol, and incubated for 30 min at 37°C with 0.1% RNase A in PBS. Cells were then washed, resuspended, and stained in PBS containing 25 μ g/ml of PI for 30 min at room temperature. Cell distribution across the cell cycle was analyzed with flow cytometry (Becton-Dickinson, Franklin Lakes, NJ). Acquisition and analysis of the data were performed using Cell Quest 3.0 software.

2.2.1 MTT assay

Cell viability was measured by an MTT assay to detect NADH-dependent dehydrogenase activity. Thirty microliters of MTT solution (2 mg/ml) in 1 \times phosphate-buffered saline (PBS) was directly added to the cells, which were then incubated for 3 h to allow MTT to metabolize to formazan. Absorbance was measured with an automated spectrophotometric plate reader at a wavelength of 570 nm. Cell viability was normalized as relative percentages in comparison with untreated controls.

2.2.2 ROS detection

Cells were collected and washed with PBS, followed by staining with 5 μ M H₂DCF-DA for 30 min. ROS generation was measured via the developed fluorescence product, dichlorofluorescein, an oxidized product of dye H₂DCF-DA. Fluorescence was measured using flow cytometry (Becton-Dickinson, Franklin Lakes, NJ). Acquisition and analysis of the data were performed using Cell Quest 3.0 software.

2.2.3 H₂O₂ and glutathione measurement

The cellular H₂O₂ and glutathione levels were measured by ROS-Glo™ H₂O₂ Assay and GSH/GSSG-Glo Assay (Promega) according to the manufacturer's protocol.

2.2.4 Cellular Glutathione Reductase (GR) determination

Cellular GR activity was measured with the Glutathione Reductase Assay kit (Abcam) according to the manufacturer's protocol.

2.2.5 Measurement of GR activity

All kinetics were carried out in GR assay buffer (50 mM potassium phosphate buffer, pH 7.6), which contains 200 mM KCl and 1 mM EDTA, at 25°C. The standard assay mixture contained 100 μ M NADPH and 0.5-1 U/ml GR. FT was allowed to react for at least 30 min before the addition of 1 mM GSSG, and the absorption decrease at 340 nm due to NADPH consumption was monitored over 3 min. Determination of the GR activity was achieved by measurement of the initial rates of disappearance of NADPH, determined spectrophotometrically at 340 nm.

2.2.6 Live/dead assay

To assess cytotoxicity, we used a live/dead assay kit (Invitrogen, Carlsbad, CA), which determines intracellular esterase activity and plasma membrane integrity. This assay uses calcein-AM, a polyanionic, green fluorescent dye that is retained within live cells, and a red fluorescent ethidium bromide homodimer dye that can enter cells through damaged membranes and bind to nucleic acids but is excluded by the intact plasma membranes of live cells.

2.2.7 Animals

All procedures involving animals were reviewed and approved by KHU Institutional Animal Care and Use Committee [KHUASP(SE)-16-007]. Five week-old athymic nu/nu female mice (NARA Biotech, Korea) were implanted subcutaneously in the right flank with U266 cells. The animals were housed (6 mice/cage) in standard mice plexi glass cages in a room maintained at

constant temperature and humidity under 12 h light and dark cycle, and fed with regular autoclaved mouse chow with water *ad libitum*. None of the mice exhibited any lesions and all tested pathogen-free. Before initiating the experiment, we acclimatized all mice to a pulverized diet for 3 days.

2.2.8 Subcutaneous implantation of U266 cells

U266 cells were harvested from sub-confluent cultures, washed once in serum-free medium, and resuspended in PBS. Only suspensions consisting of single cells, with >90% viability, were used for the injections. U266 cells [$1 \times 10^7/100 \mu\text{L}$ PBS:Matrigel (1:1)] were injected subcutaneously into the right flank of the mice. To prevent leakage, a cotton swab was held cautiously for 1 minute over the site of injection.

2.2.9 Experimental protocol

When tumors reached 0.5 cm in diameter, the mice were randomized into the following treatment groups ($n = 6/\text{group}$). Group I was given PBS (200 μL , i.p. thrice/week), group II was given FT (20 mg/kg body weight, i.p. thrice/week), group III was given FT (40 mg/kg body weight, i.p. thrice/week). Therapy was continued for 20 days, and the animals were euthanized 1 week later. Primary tumors were excised and the final tumor volume was measured as $V = 4 / 3 \pi r^3$, where r is the mean radius of the three dimensions (length, width, and depth). Half of the tumor tissue was fixed in formalin and embedded in paraffin for immunohistochemistry. The other half was snap frozen in liquid nitrogen and stored at -80°C .

2.3 Immunohistochemical analysis of MM tumor samples

Solid tumors from control and treatment groups were fixed with 10% phosphate buffered formalin, processed, and embedded in paraffin. Sections were cut and deparaffinized in xylene, dehydrated in graded ethanols, and finally hydrated in water. Antigen retrieval was performed by boiling the slide in 10 mM sodium citrate (pH 6.0) for 30 min. Immunohistochemistry was performed following the manufacturer's instructions (Vector Laboratories ImmPRESSTM REAGENT KIT). Briefly, endogenous peroxidases were quenched with 3% hydrogen peroxide. Non-specific binding was blocked by incubation in the blocking reagent in the ImmPRESSTM REAGENT KIT (Vector Laboratories, Burlingame, CA) according to the manufacturer's instructions. Sections were incubated overnight with primary antibodies as follows: anti-Ki-67, anti-CD31, anti-p-STAT3(Tyr705), anti-p-STAT5(Tyr 694/Tyr 699), and anti-GSH (each at 1:100 dilutions). Slides were subsequently washed several times in PBS and were incubated with ImmPRESSTM reagent according to the manufacturer's instructions. Immunoreactive species were detected using 3, 3'-diaminobenzidine tetrahydrochloride (DAB) as a substrate. Sections were counterstained with Gill's hematoxylin and mounted under glass coverslips. Images were taken using an Olympus BX51 microscope (magnification, 20 \times).

2.3.1 GSH level analysis in tumor tissues

Tumor tissues were homogenized in 5% metaphosphoric acid (0.1 g/ml tissue), and then centrifuged at $16,000 \times g$ at 4°C for 15 min. Supernatants were collected and analyzed for GSH content using a GSH/GSSG ratio assay kit (Abcam, Cambridge, MA) as per the manufacturer's protocol.

2.3.2 Western blot analysis for tumor tissues

MM tissues (75-100 mg) from control and experimental mice were minced and incubated on ice for 30 minutes in 0.5 ml of ice-cold T-PER Tissue Protein Extraction Reagent (Pierce, Rockford, USA). The minced tissue was centrifuged at $16,000 \times g$ at 4°C for 20 minutes. The proteins were then fractionated by SDS-PAGE, electrotransferred to nitrocellulose membranes, blotted with each antibody, and detected by enhanced chemiluminescence (ECL) kit (GE Healthcare, Waukesha, USA).

2.3.3 Statistical analysis

All numeric values are represented as the mean \pm SE. Statistical significance of the data compared with the untreated control was determined using the Mann-Whitney U test. Significance was set at $P < 0.05$.

3. Results

3.1.1 FT inhibits the STAT activation cascade in MM cells.

To investigate the potential effect of FT on the STAT signaling pathway, we used diverse molecular biology techniques. Previous studies have shown that STAT is a key point of multiple oncogenic signaling pathways [33, 60, 61]. We first analyzed whether FT inactivated STAT3 in U266 cells by detecting p-STAT3(Tyr705) and p-STAT3(Ser727) levels using Western blot analysis. As shown in Fig. 1B, we found that both constitutive p-STAT3(Tyr705) and p-STAT3(Ser727) levels were substantially reduced upon FT treatment in a dose- and time-dependent manner. However, FT had no effect on the expression of STAT3 protein (Fig. 1B, *third panel*). Whether FT inhibits the activation of another STAT family isoform, STAT5 in U266 cells was also investigated. We noticed that FT substantially reduced STAT5 activation in a dose- and time-dependent manner, without affecting total STAT5 levels, as analyzed by Western blot analysis (Fig. 1B, *fourth and fifth panel*).

3.1.2 FT reduces binding capacity of STAT3 and STAT5 to the DNA.

Because tyrosine phosphorylation causes the dimerization of STATs and their translocation to the nucleus, where they bind to DNA and regulate gene transcription [13, 61, 62], we analyzed whether FT can reduce the DNA-binding ability of STAT3 and STAT5. EMSA analysis of nuclear extracts prepared from U266 cells showed that FT reduced STAT3 and STAT5-DNA binding activities in a dose- and time-dependent manner (Fig. 1C and D). These results show that FT abrogates the DNA binding ability of STAT3 and STAT5.

3.1.3 FT down-modulates the nuclear pool of p-STAT3 and p-STAT5 in U266 cells.

Because the active dimer of STATs is capable of translocating to the nucleus and inducing transcription of specific target genes [61, 62], we next analyzed whether FT can suppress nuclear translocation of p-STAT3 and p-STAT5. Using immunocytochemistry, Fig. 1E and F clearly demonstrate that FT reduced the translocation of p-STAT3 and p-STAT5 to the nucleus in U266 cells.

3.1.4 FT inhibits activation of upstream kinases involved in the STAT3 signaling cascade in MM cells.

Janus kinases (JAK) and Src families are the major upstream tyrosine kinases that can regulate STAT3 activation [33]. In order to determine which upstream signaling molecules are involved in FT-mediated STAT3 inactivation, we examined the effects of FT on the phosphorylation of JAK1, JAK2, and Src in U266 cells. As shown in Fig. 1G, JAK1 and JAK2 was constitutively active in U266 cells, and treatment with FT clearly reduced the phosphorylation in a dose- and time-dependent manner. The expression levels of total JAK1 and JAK2 remained unchanged under the same treatment conditions (Fig. 1G, *second and fourth panel*). Previous studies have shown that STAT3 is activated by soluble tyrosine kinases of the Src kinase families [63]. Accordingly, we next conducted a study the effect of FT on constitutive activation of Src kinase in U266 cells. FT downregulated the activation of Src kinase in a concentration- and time-dependent manner in MM cells (Fig. 1G).

3.1.5 FT reduces inducible STAT3/5 and upstream kinases of STAT3 in RPMI 8226 cells.

To investigate IL-6-mediated intracellular signaling, we first detected STAT3 phosphorylation in RPMI 8226 cells. As shown in Fig. 2A, IL-6 activated phosphorylation of STAT3(Tyr705), and the response peaked at 15 min, then decreased. We next determined whether FT could also inhibit IL-6-induced STAT3/5 phosphorylation in RPMI 8226 cells that display relatively low levels of constitutively active STAT3/5. Interestingly, we observed that IL-6-induced STAT3 as well as STAT5 phosphorylation was suppressed by FT in a time-dependent manner. Exposure of cells to FT for 6 h was sufficient to substantially suppress IL-6-induced STAT3(Tyr705 and Ser727) and STAT5 phosphorylation in RPMI 8226 cells (Fig. 2B). Also, we found that FT can abrogate IL-6 induced JAK1/2 and Src phosphorylation in RPMI 8226 cells (Fig. 2C). These results clearly suggest that FT can also downregulate inducible STAT3/5 activation in MM cells.

3.1.6 FT suppresses IL-6-induced STAT3-dependent reporter gene expression.

Our results up to this point showed that FT inhibited the phosphorylation, nuclear translocation, and DNA binding activity of STAT3. We next determined whether FT affects STAT3-dependent gene transcription. When cells transiently transfected with the p-STAT3-Luc construct were stimulated with IL-6, STAT3-mediated luciferase gene expression significantly increased. Dominant-negative STAT3 blocked this increase, indicating specificity. When the cells were pretreated with FT, IL-6-induced STAT3 activity was inhibited in a dose-dependent manner (Fig. 2D).

3.1.7 Ectopic expression of STAT3 rescued FT-induced inhibition of cell viability.

To further confirm if the abrogation of STAT3 activation was crucial in FT-mediated inhibition of cell viability, U266 cells were transiently transfected with a STAT3C-expressing construct before FT treatment. Western blotting data showed that transient transfection of the STAT3C-expressing construct in U266 cells resulted in a remarkable increase in STAT3 and p-STAT3(Tyr705) expression (Fig. 2E). As expected, upon the overexpression of STAT3 in U266 cells, the observed inhibitory effect of FT on cell viability was rescued as compared to the cells transfected with the empty vector alone (Fig. 2F).

3.1.8 FT downregulates the expression of various proteins involved in anti-apoptosis, angiogenesis, and proliferation.

Because Bcl-2, Survivin, and IAP-2 have been associated with apoptosis and mitochondrial malfunction, we next examined the effects of FT on the constitutive expression of these mRNA and proteins. As shown in Fig 3A and 3B, we found that FT downregulates the expression of anti-apoptotic mRNA levels and gene products, and proteins linked with cell angiogenesis (VEGF) in a dose-dependent manner. Also, FT repressed the expression of cell proliferation proteins (CDK2, CDK4, and Cyclin E) (Fig. 3C).

3.1.9 FT activates caspase-3 and causes PARP cleavage in U266 cells.

In order to investigate the effect of FT on apoptosis induction, caspase-3 activation was examined by Western blot analysis. As shown in Fig. 3D first panel, we found a substantial dose-dependent activation of caspase-3 by FT in U266 cells. Activation of downstream caspase led to the cleavage of a 116 kDa PARP protein into 87 kDa fragments (Fig. 3D, *second panel*).

3.2 FT negatively affects the cell cycle in MM cells.

We next tried to determine the effect of FT on cell cycle progression in U266 and RPMI 8226 cells. After FT treatment for 24 h, cells were labeled with PI and analyzed by flow cytometry. As shown in Fig. 3E, FT induced an increased accumulation of the cell population in sub-G1 phase contents to 21 % at 100 μ M of FT, compared to untreated control (3 %) in U266 cells. In RPMI 8226 cells, accumulation of the S phase cell population increased to 15 %, compared to untreated control (8 %), and G2 phase cells increased from 21% to 32%.

3.2.1 FT reduces the expression of Cyclin D1 and Cyclin B1 associated with cell cycle regulation.

Since the cell cycle arrest effects by FT were different in U266 and RPMI 8226 cells, we conducted additional experiments to address this issue. Because Cyclin D1 is associated with sub-G1 phase [64] and Cyclin B1 is known to be linked with G2/M phase [65], we next examined the effects of FT on the expression of these proteins by Western blotting. As shown in Fig. 3F, we found that FT downregulates the expression of Cyclin D1 (U266) and Cyclin B1 (RPMI 8226) in a dose-dependent manner.

3.2.2 FT inhibits cell viability in MM cells.

To clearly investigate the effects of FT on U266 and RPMI 8226 cell viability, the cells were treated with 50, 75, or 100 μ M concentrations of FT, and then cell viability was analyzed using an MTT assay. As shown in Fig. 3G, FT significantly suppressed cell viability in MM cells in a time- and dose-dependent manner. In addition, to compare the cytotoxicity of FT to healthy cells, MTT assay for PBMC was performed. As shown in Fig. 3H, FT significantly inhibited the viability of U266 cells in a dose-dependent manner, but not of PBMC. The results indicate that inhibition of cell viability by FT may be cell type-specific.

3.2.3 Antioxidants reverse FT-induced STAT3 inhibition and cellular apoptosis.

N-acetyl-L-cysteine (NAC) and glutathione (GSH) are two major thiol-related antioxidants [66, 67]. Interestingly, pretreatment of U266 cells with these two antioxidants substantially abolished STAT3 abrogation caused by FT treatment (Fig. 4A and 4B), thereby indicating that oxidative stress may be involved in the inhibitory effect of FT on STAT3 in U266 MM cells. Furthermore, NAC/GSH pretreatment was also found to significantly reduce cellular apoptosis induced by FT, as observed by Western blot analyses (Fig. 4C and 4D) and flow cytometry (Fig. 4E), further demonstrating that oxidative stress may also contribute to the observed pro-apoptotic effects of FT.

3.2.4 GSH/GSSG imbalance contributes to FT-induced reactive oxygen species production.

To further validate whether FT can induce oxidative stress in MM cells, reactive oxygen species (ROS) levels were measured in U266 cells by staining with H₂DCF-DA. We observed a significant increase of ROS production upon FT treatment (Fig. 5A), but not in PBMC (Fig. 5B), suggesting that FT can indeed induce oxidative stress in MM cells.

The GSH/GSSG system is one of the major intracellular antioxidant systems [68]. The ratio of GSH to oxidized glutathione (GSSG) is an indicator of cellular oxidative stress [69]. To explore the possible mechanism(s) of increased ROS production, we analyzed the effect of FT on the GSH/GSSG system. As shown in Fig. 5C and D, a significant decrease of GSH and an obvious increase of GSSG were observed in U266 cells upon treatment, thereby indicating that exposure of the cells to the drug resulted in an imbalance of the GSH/GSSG system. In addition, an almost twofold elevation of the GSSG/GSH ratio was observed (Fig. 5E), demonstrating that FT can induce oxidative stress in U266 cells. To further investigate the role of GSH/GSSG imbalance in mediating FT-induced oxidative stress, both the GSH synthesis blocker buthionine sulfoximine (BSO) and GSH prodrug NAC were employed. We found that pretreatment with NAC significantly prevented FT-induced ROS production, while BSO enhanced ROS production (Fig. 5F).

To further clarify the type of ROS involved, we measured the H₂O₂ level in FT treated cells. As shown in Fig. 5G, a dose-dependent increase of H₂O₂ was observed, compared to untreated control. Like the general ROS, increased H₂O₂ production was also prevented by NAC and enhanced by BSO (Fig. 5H). These results demonstrate that H₂O₂ is the major ROS induced by FT in MM cells.

In addition, BSO enhanced FT-induced cellular apoptosis when applied in combination with FT, and the increased apoptosis could also be attenuated by NAC pretreatment (Fig. 5I), providing strong evidence(s) that GSH/GSSG imbalance primarily contributes to the FT-induced oxidative stress and its observed anti-cancer effects in U266 cells.

3.2.5 FT inhibits the glutathione reductase protein expression in U266 cells

Glutathione reductase (GR) catalyzes the reduction of GSSG to GSH to resist oxidative stress [70]. As we observed a significant alteration in the GSH/GSSG ratio, we next investigated whether this imbalance may be due to a disturbance in GR activity. We treated the cells with FT and collected the cell homogenates to measure cellular GR activity. A dose-dependent reduction of GR activity was observed (Fig. 6A). Furthermore, we next examined the effects of FT on the expression of GR protein. As shown in Fig 6B, we found that FT downregulates the expression of the GR protein, indicating that GR inhibition by FT is mediated through negative regulation of its protein expression.

To clarify how FT downregulates GR, we next investigated the interaction between GR and FT in a cell-free assay system. GR was incubated with FT in the presence of NADPH for 30 min, and then the substrate GSSG was added to initiate the reaction. As shown in Fig. 6C, no change was observed in the GR activity on FT treatment. These results demonstrate that FT directly suppresses GR by inhibiting its protein activity.

3.2.6 FT potentiates the STAT3 inhibitory effects of chemotherapeutic drugs in MM cells..

Bortezomib (Bor) is the most effective anticancer drug used in the treatment of variety of cancers. To determine whether FT potentiates the apoptotic effect of anticancer drug, we treated U266 cells with FT combined with Bor, and then examined the Western blotting and Live/dead assays. FT and Bor combination treatment suppressed the p-STAT3 (Tyr705), p-STAT3(Ser727), and p-

STAT5 (Tyr 694/Tyr 699) in U266 cells and had no effect on the expression of total STAT3 and STAT5 protein in whole-cell protein lysates (Fig. 6D). Furthermore, we found that combination treatment enhanced U266 cell death as compared to the individual treatment (Fig. 6E), thereby indicating that FT can indeed potentiate drug-induced apoptosis.

3.2.7 FT induces anti-tumor effects in a xenograft MM model.

We examined the therapeutic potential of FT on the growth of subcutaneously implanted human MM U266 cells in nude mice. The experimental protocol is depicted in Fig. 7A. U266 cells were implanted subcutaneously in the right flank of nude mice. When tumors have reached 0.5 cm in diameter after a week, the mice were randomized into 3 groups and the treatment was commenced as per the experimental protocol. The tumor diameters were measured at 4-day intervals. The treatment was continued for 3 weeks and animals were sacrificed after 4 weeks. The tumors were excised, and the tumor diameters were measured. We found that the tumor volume increased rapidly in the control group compared with the other treatment groups (Fig. 7B). We found that FT, when given at 40 mg/kg body weight, considerably inhibited the growth of the tumor at Day 24 after treatment (Fig. 7C and D). Mice body weights increased during the drug treatment period (Fig. 7E).

3.2.8 FT suppresses the growth of human MM *in vivo* and inhibits STAT3/5 activation from tumor tissues.

We also tested the anti-tumor potential of FT *in vivo* via intraperitoneal administration in a subcutaneous model of human MM xenograft in nude mice. We evaluated the effect of FT on constitutive p-STAT3 and p-STAT5 levels in MM tumor tissues by immunohistochemical analysis and found that FT significantly downregulated the expression of p-STAT3/5 in tumor tissues compared with the control group (Fig. 8A). Furthermore, to determine whether FT decreases MM tumor growth by inhibiting proliferation, we examined the expression of Ki-67+ cells in MM tumors from mice. A Ki-67+ index was used as a marker for cell proliferation. Our results showed that FT decreased the expression of Ki-67 in tumor tissues in a dose-dependent manner (Fig. 8B, *upper panel*). Also, to evaluate whether FT suppresses MM tumor growth by inhibiting angiogenesis, we examined the expression of the microvessel density marker CD31+ in MM tumors from nude mice. Our results showed that FT significantly reduced the microvessel density. (Fig. 8B, *lower panel*). In addition, we performed immunohistochemical analysis to examine the expression levels of GSH by FT, and confirmed the decrease in the expression level of GSH in MM tumor tissues (Fig. 8C).

3.2.9 FT reduces the levels of GSH in tumor tissues.

The effect of FT on the GSH content in MM tumor tissues was also measured. The data showed that the GSH level was significantly decreased (~50% decrease) in the 40 mg/kg of FT treatment group compared to the vehicle group (Fig. 8D), which is in line with the cell line data where the cellular GSH content was reduced upon FT treatment.

3.3 FT abrogates the activation of STAT3 and STAT5 in tumor tissues.

We also investigated the effect of FT on phosphorylation level of STAT3 (Tyr705 and Ser727) and STAT5 in MM tumor tissues. Fig. 8 D showed that FT was quite effective in suppressing the expression of p-STAT3 (Tyr705), p-STAT3(Ser727), and p-STAT5 in a concentration-dependent manner.

3.3.1 FT activates caspase-3 and causes PARP cleavage in MM tumor tissues.

In order to evaluate the effect of FT on apoptosis induction in tumor tissues; caspase-3 activation and PARP cleavage was examined by Western blot analysis. As shown in Fig. 8E *first panel*, we found a substantial concentration-dependent activation of caspase-3 by FT in MM tumor tissues. Activation of downstream caspase led to the cleavage of a 116 kDa PARP protein into 87 kDa fragments (Fig. 8E, *second panel*).

3.3.2 FT down-regulates expression of various proteins involved in apoptosis in tumor tissues.

Next, we examined whether FT can down-modulate the expression of anti-apoptotic proteins in tumor tissues, which was determined by Western blot analysis. We found that FT suppressed the expression of Bcl-2, Bcl-xL, Survivin, IAP-1, and VEGF in a concentration-dependent manner (Fig. 8F).

4. Discussion

We found that FT exerted its potent inhibitory effects on both constitutive and IL-6-inducible STAT3 (tyrosine residue 705 and serine residue 727) and STAT5 (tyrosine residue 694 and 699) activation in MM cells, concomitant with the inhibition of JAK1, JAK2, and c-Src activation. We further found that FT also modulated the GSH/GSSG system and thereby caused oxidative stress that mediated its observed STAT3 inhibitory effects in MM cells. FT further down-regulated the expression of various STAT3-regulated gene products, caused inhibition of cell proliferation, induced substantial apoptosis, and induced significant suppression of the growth of MM in a xenograft mouse model.

We first noted that FT could suppress constitutive STAT3 (both at Tyr705 and Ser727 residue) and STAT5 phosphorylation (Tyr 694/Tyr 699 residue), in U266 multiple myeloma cells. Also, we observed that FT inhibited the DNA-binding affinity and nuclear translocation of both STAT3 and STAT5. Next, how FT affects the STAT3 and STAT5 signaling pathway was also investigated in detail. The activation of JAK has been closely linked with STAT3 and STAT5 activation [13] and we observed that FT inhibited the activation of constitutively active JAK1, JAK2, and Src in U266 MM cells. JAKs are essential for the tyrosine phosphorylation of STAT3 in response to growth factors and cytokines [71]. STAT3 and STAT5 phosphorylation clearly plays a pivotal role in the proliferation and survival of a wide variety of tumor cells, and blockade of JAK/STATs signals can provide a potent therapeutic strategy for MM [32, 36, 72]. We further observed that FT could also inhibit IL-6-induced STAT3/5 and its upstream protein tyrosine kinase (JAK1, JAK2, and Src) phosphorylation in RPMI 8226 cells in a time-dependent manner that display relatively low levels of constitutively active STAT3/5.

We also found evidence that FT can downregulate the expression of several STAT3-regulated genes; including anti-apoptotic gene products (Bcl-2, Survivin, and IAP-2), inducers of angiogenesis (VEGF), and cell proliferation and cell-cycle regulators (CDK2, CDK4, and cyclin E). Constitutively active STAT3/5 is closely associated with oncogenesis by protecting cancer cells from apoptosis [73], possibly through the expression of Bcl-2, Survivin, and IAP-2 [74-76]; this means that inhibition of STAT3/5 activation by agents such as FT could promote apoptosis. The inhibition of cyclin E expression by FT correlated with suppression in proliferation and arrest of the cell cycle. Bcl-2 can also obstruct cell death induced by a variety of chemotherapeutic agents, in parallel with an increase in chemoresistance [77]. The down-regulation of the expression of Bcl-2, Survivin, and IAP-2 is likely linked with the ability of FT to induce apoptosis in MM cells. Also, our findings are in part agreement with a recent study in which FT was found to induce apoptosis in human non-small cell lung cancer via induction of cell cycle arrest [52], and in a human osteosarcoma cell line by regulating the expression of Bcl-2, Bax, and MiR-375 [78]; although its detailed mechanism of action was not investigated in this report.

Interestingly, we found that the FT-induced cellular apoptosis as well as STAT3/5 abolishment could be reversed by the ROS scavengers, NAC and GSH. Under normal physiological conditions, ROS remain at physiological levels and perform the function of anti-oxidative systems [79, 80]. In general, low levels of ROS contribute to cell survival and proliferation. However, when ROS accumulate at elevated non-physiological concentrations, they can lead to apoptotic cell death through damage of cellular macromolecules such as DNA and proteins [81]. We hypothesized that both FT-induced STAT3 inhibition and apoptosis were abolished by ROS scavengers, suggesting that ROS may be involved in STAT3 inhibition and anti-cancer effects of FT. We definitely observed a significant increase of ROS (to be specific, H_2O_2) in MM cells upon FT treatment, supporting our hypothesis that FT can induce ROS production in U266 MM cells. The capability of FT to induce ROS production was further demonstrated by the twofold increase of the GSSG/GSH ratio, which is an indicator of cellular oxidative stress. Increased ROS production by FT can be caused by an imbalance of the GSH/GSSG system. The disruption of this system will limit its ability to remove ROS and result in increased ROS production. We observed a significant GSH decrease and a GSSG increase in FT-treated cells compared to untreated cells, suggesting that FT treatment actually interfered with the GSH/GSSG system. GSH decrease was also observed in the mouse tumor tissue obtained 24 days after treatment with FT (Fig. 8C). In addition, supplementation of GSH with NAC abrogated FT-induced ROS/ H_2O_2 production and apoptosis, while inhibition of GSH synthesis by BSO showed the opposite effects. These glutathione system disturbances contribute to FT-induced ROS production and anti-cancer effects.

Next, we measured the GR activity by FT, since the inhibition of GR by FT may cause an imbalance of GSH/GSSG, and we observed a significant GR reduction by FT treatment. The GSH levels can be supplemented by GR, which acts to catalyze the conversion of GSSG to GSH [80]. GR kinetic activity was not inhibited by FT when incubated with the substrates NADPH and GSSG. GR inhibition may be due to a reduction in the GR activity, as we observed a reduction in GR protein expression.

We also analyzed potential effects of FT administration on tumor growth in a xenograft mouse model. FT significantly suppressed MM growth, down-regulated the expression of phospho-STAT3/STAT5, and increased the levels of caspase-3 in FT treated group as compared with control. Immunohistochemical analysis of tumor tissues indicated that this isoflavone exerted its *in vivo* anti-cancer effects by down-modulating p-STAT3 and p-STAT5 expression, which correlates well with its observed *in vitro* effects. The down-modulation of Ki-67 and CD31 expression in tumor tissues by FT also emphasized the anti-proliferative and anti-angiogenic potential of FT in MM, an aspect which requires further detailed investigation. Moreover, no prior studies with FT have been reported using a MM mouse model, and our findings clearly indicate that FT has definite potential for the treatment of MM through the suppression of the STAT3/STAT5 activation.

Overall, our *in vitro* and *in vivo* experimental observations clearly indicate that the anti-cancer effects of FT in human MM are mediated through the suppression of the STAT3 and STAT5 activation cascade and its-regulated oncogenic gene products. Taken together, these results provide a strong rationale for pursuing the use of FT to enhance treatment efficacy in MM patients.

5. Acknowledgements

This work was supported by the National Research Foundation of Korea (NRF) grant funded by the Korean Government (MSIP) (NRF-2015R1A4A1042399, 2016R1A6A3A11932713, and 2017M3A9E4065333)

6. Conflict of interest statements

The authors have no conflicts of interest to disclosure.

7. Figure legends

Fig. 1. FT shows dose- and time-dependent inhibition of STAT3 and STAT5 phosphorylation in MM. (A) The chemical structure of Formononetin (FT). (B) U266 cells (1×10^6 cells/well) were seeded onto 6-well plates, incubated at 37°C with various indicated concentrations of FT for 6 h (*left panel*), and treated with $100 \mu\text{M}$ of FT for various time intervals (*right panel*). Thereafter, equal amounts of lysates were analyzed by Western blot analysis using antibodies against p-STAT3 (Tyr705), p-STAT3(Ser727), STAT3, p-STAT5(Tyr694/Tyr699), and STAT5. The same blots were stripped and reprobated with β -actin antibody to verify equal protein loading. The results shown here are representative of three independent experiments. Image J was employed to quantify the relative expression of p-STAT3 (Tyr705), p-STAT3(Ser727), and p-STAT5(Tyr694/Tyr699) normalized to the β -actin loading control (optical density). Data are shown as the mean \pm SD (** $P < 0.01$, *** $P < 0.001$). (C and D) FT suppresses STAT3 and STAT5 binding activity in U266 cells. After U266 cells (1×10^6 cells/well) were seeded onto 6-well plates, incubated at 37°C with the indicated concentrations of FT for 6 h (*left panel*) and treated with $100 \mu\text{M}$ of FT for various time intervals (*right panel*), they were analyzed for nuclear STAT3 and STAT5 levels by EMSA. The results shown here are representative of three independent experiments. Image J was employed to quantify the relative expression of STAT3 and STAT5 normalized to the drug-treated/control groups. β -actin loading control (optical density). Data are shown as the mean \pm SD (** $P < 0.01$, *** $P < 0.001$). (E and F) FT causes inhibition of translocation of STAT3 and STAT5 to the nucleus. After 6 h of FT treatment, the cells were fixed and permeabilized. p-STAT3 (green) was immunostained with Alexa Fluor[®] 488 donkey anti-goat IgG (H+L) antibody, STAT3 (red) was immunostained with Alexa Fluor[®] 594 donkey anti-rabbit IgG (H+L) antibody, and the nuclei (blue) were stained with DAPI. The fourth panels show the merged images of the first, second, and third panels. The results shown are representative of two independent experiments. (G) U266 cells (1×10^6 cells/well) were seeded onto 6-well plates, incubated at 37°C with various indicated concentrations of FT for 6 h (*left panel*), and treated with $100 \mu\text{M}$ of FT for various time intervals (*right panel*). Thereafter, equal amounts of lysates were analyzed by Western blot analysis using antibodies against p-JAK1(Tyr1022/1023), JAK1, p-JAK2 (Tyr1007/1008), JAK2, p-Src(Tyr416), and Src. The same blots were stripped and reprobated with β -actin antibody to verify equal protein loading. The results shown here are representative of three independent experiments. Image J was employed to quantify the relative expression of p-JAK1 (Tyr1022/1023), p-JAK2(Tyr1007/1008), and p-Src(Tyr416) normalized to the β -actin loading control (optical density). Data are shown as the mean \pm SD (** $P < 0.01$, *** $P < 0.001$).

Fig. 2. FT inhibits inducible STAT3/5 and upstream kinases of STAT3 in RPMI 8226 cells. (A) RPMI 8226 cells (1×10^6 cells/well) were treated with IL-6 (10 ng/mL) for the indicated time intervals, and whole-cell extracts were prepared. Thereafter, equal amounts of lysates were analyzed by Western blot analysis using antibodies against p-STAT3(Tyr705) and STAT3. The same blots were stripped and reprobated with β -actin antibody to verify equal protein loading. Image J was employed to quantify the relative expression of p-STAT3 (Tyr705) normalized to the β -actin loading control (optical density). Data are shown as the mean \pm SD (*** $P < 0.001$). (B and C) RPMI 8226 cells (1×10^6 cells/well) were treated with $100 \mu\text{M}$ of FT for the indicated times and then stimulated with IL-6 (10 ng/mL) for 15 min. Whole-cell extracts were prepared and equal amounts of lysates were analyzed by Western blot analysis using antibodies against p-STAT3(Tyr705), p-STAT3(Ser727), STAT3, p-STAT5(Tyr694/Tyr699), STAT5, p-JAK1(Tyr1022/1023), JAK1, p-JAK2(Tyr1007/1008), JAK2, p-Src(Tyr416), and Src. The same blots were stripped and reprobated with β -actin antibody to verify equal protein loading. The results shown here are representative of three independent experiments. Image J was employed to quantify the relative expression of p-STAT3(Tyr705), p-STAT3(Ser727), p-STAT5(Tyr694/Tyr699), p-JAK1(Tyr1022/1023), p-JAK2(Tyr1007/1008), and p-Src(Tyr416) normalized to the β -actin loading control (optical density). Data are shown as the mean \pm SD (** $P < 0.01$, *** $P < 0.001$). (D) RPMI 8226 cells (1×10^6 cells/well) were transfected with STAT3-luciferase (STAT3-Luc) plasmid, incubated for 48 h, and treated with 50, 75, and $100 \mu\text{M}$ of FT for 6 h and then stimulated with IL-6 (10 ng/mL) for 15 min. Whole-cell extracts were then prepared and analyzed for luciferase activity. The results shown are representative of three independent experiments. (E) U266 cells were transiently transfected with STAT3-C Flag pRc/CMV or empty vector plasmids. Then, equal amounts of lysate were analyzed by Western blot analysis using antibodies against p-STAT3(Tyr705), Flag, and STAT3. The same blots were stripped and reprobated with β -actin antibody to verify equal protein loading. Image J was employed to quantify the relative expression of p-STAT3(Tyr705) normalized to the β -actin loading control (optical density). (F) U266 cells were transiently transfected with STAT3-C Flag pRc/CMV or empty vector plasmids. Then, after the transient transfection U266 cells (1×10^4 cells/well) were seeded into 96-well plates, treated with indicated concentrations of FT for 24 h. The cell viability was thereafter measured using MTT assay.

Fig. 3. FT induces apoptosis, causes accumulation of the cell cycle, and suppresses cell proliferation in MM cells. (A) U266 cells (1×10^6 cells/well) were seeded onto 6-well plates, incubated at 37°C with various indicated concentrations of FT for 24 h. Thereafter, equal amounts of lysates were analyzed by Western blot analysis using antibodies against Bcl-2, Survivin, IAP-2, and VEGF. The same blots were stripped and reprobated with β -actin antibody to verify equal protein loading. The results shown here are representative of three independent experiments. Image J was employed to quantify the relative expression of Bcl-2, Survivin, IAP-2, and VEGF normalized to the β -actin loading control (optical density). Data are shown as the mean \pm SD (** $P < 0.01$). (B) U266 cells (1×10^6 cells/well) were treated with indicated concentrations of FT for 24 h. Total RNA was isolated, Bcl-2 and Survivin mRNA expression was examined by RT-PCR analysis. GAPDH was performed to control for a similar initial cDNA content of the sample. The results shown are representative of three independent experiments. Image J was employed to quantify the relative expression of Bcl-2 and Survivin normalized to the GAPDH loading control (optical density). Data are shown as the mean \pm SD (*** $P < 0.001$).

(C and D) Cells (1×10^6 cells/well) were seeded onto 6-well plates and treated with various indicated concentrations of FT for 24 h. Whole-cell extracts were prepared, equal amounts of lysates were analyzed by Western blot analysis, and then probed with antibodies against CDK2, CDK4, Cyclin E, caspase-3, and PARP as described in the Materials and methods. The same blots were stripped and reprobed with β -actin antibody to verify equal protein loading. The results shown here are representative of three independent experiments. Image J was employed to quantify the relative expression of CDK2, CDK4, Cyclin E, cleaved caspase-3, and cleaved PARP normalized to the β -actin loading control (optical density). Data are shown as the mean \pm SD (** $P < 0.01$, *** $P < 0.001$). (E) U266 and RPMI 8226 cells (1×10^6 cells/well) were treated with 100 μ M of FT for 24h. Then, the cells were fixed and analyzed using flow cytometry. The results shown here are representative of three independent experiments. (F) U266 and RPMI 8226 cells (1×10^6 cells/well) were seeded onto 6-well plates, incubated at 37 $^{\circ}$ C with various indicated concentrations of FT for 24 h. Thereafter, equal amounts of lysates were analyzed by Western blot analysis using antibodies against Cyclin D1 and Cyclin B1. The same blots were stripped and reprobed with β -actin antibody to verify equal protein loading. The results shown here are representative of three independent experiments. Image J was employed to quantify the relative expression of Cyclin D1 and Cyclin B1 normalised to the β -actin loading control (optical density). Data are shown as the mean \pm SD (** $P < 0.01$, *** $P < 0.001$). (G) After U266 and RPMI 8226 cells (1×10^4 cells/well) were seeded onto 96-well plates, they were left non-treated (NT, \bullet), treated with FT at 50 μ M (\circ), 75 μ M (\blacktriangledown), and 100 μ M (\blacktriangle) for the indicated time intervals. The cell viability was measured using an MTT assay. (H) After U266 and PBMC (1×10^4 cells/well) were seeded onto 96-well plates, they were treated with indicated concentrations of FT for 24 h. The cell viability was measured using MTT assay.

Fig. 4. NAC and GSH reverse the STAT3 inhibition and apoptosis induced by FT. (A and B) U266 cells (1×10^6 cells/well) were pretreated with indicated concentrations of NAC or GSH for 30 min, and then exposed to FT (100 μ M) for 6 h. Whole cell extracts were prepared and subjected to Western blot analysis using antibodies against p-STAT3 (Tyr705) and STAT3. The same blots were stripped and reprobed with β -actin antibody to verify equal protein loading. The results shown here are representative of three independent experiments. Image J was employed to quantify the relative expression of p-STAT3 (Tyr705) normalised to the β -actin loading control (optical density). Data are shown as the mean \pm SD (** $P < 0.01$, *** $P < 0.001$). (C and D) U266 cells (1×10^6 cells/well) were pretreated with NAC (5 mM) or GSH (2.5 mM) for 30 min, and then exposed to FT (100 μ M) for 24 h. Thereafter, whole cell extracts were prepared and subjected to Western blot analysis using specific antibodies for the indicated proteins. The results shown are representative of at least three independent experiments. Image J was employed to quantify the relative expression of cleaved caspase-3, and cleaved PARP normalized to the β -actin loading control (optical density). Data are shown as the mean \pm SD (** $P < 0.001$). (E) U266 cells (1×10^6 cells/well) were pretreated with NAC (5 mM) or GSH (2.5 mM) for 30 min, and then exposed to FT (100 μ M) for 24 h. Then, the cells were fixed and analyzed using flow cytometry. The results shown here are representative of three independent experiments.

Fig. 5. GSH/GSSG imbalance mediates the FT-induced ROS production. (A) U266 cells (1×10^6 cells/well) were treated with indicated concentrations of FT for 24h. Then, the cells were incubated at 37 $^{\circ}$ C with H₂DCF-DA for 30 min and analyzed using flow cytometry. The results shown here are representative of three independent experiments. (B) PBMC (1×10^6 cells/well) were treated with 100 μ M of FT for 24h. Then, the cells were incubated at 37 $^{\circ}$ C with H₂DCF-DA for 30 min and analyzed using flow cytometry. The results shown here are representative of three independent experiments. (C-E) U266 cells (5×10^3 cells/well) were treated with indicated concentrations of FT for 24 h, and then assayed for GSH, GSSG, and GSSG/GSH with a GSH/GSSG-Glo Assay kit, as described in the Materials and Methods section. (F) U266 cells were exposed to BSO (250 μ M) with or without NAC (5 mM) for 30 min, and then treated with FT (100 μ M) for 24 h. The cells were incubated at 37 $^{\circ}$ C with H₂DCF-DA for 30 min and analyzed using flow cytometry. The results shown here are representative of three independent experiments. (G) U266 cells (1×10^4 cells/well) were treated with indicated concentrations of FT for 24 h and then subjected to assay for H₂O₂ analysis. (H) U266 cells (1×10^4 cells/well) were pretreated with or without BSO (250 μ M) or NAC (5 mM) for 30 min, and then treated with FT (100 μ M) for 24 h. The cells were then subjected to assay for H₂O₂ analysis. H₂O₂ levels were expressed as the value relative to the untreated cells. (I) U266 cells were exposed to BSO (250 μ M) with or without NAC (5 mM) for 30 min, and then treated with FT (100 μ M) for 24 h. The cells were fixed and analyzed using flow cytometry. The results shown here are representative of three independent experiments.

Fig. 6. FT directly suppresses GR activity. (A) U266 cells (1×10^6 cells/well) were exposed to indicated concentrations of FT for 24 h, and then collected for investigation using a cellular GR assay kit following the manufacturer's instructions. (B) U266 cells (1×10^6 cells/well) were seeded onto 6-well plates, incubated at 37 $^{\circ}$ C with various indicated concentrations of FT for 24 h. Thereafter, equal amounts of lysates were analyzed by Western blot analysis using antibodies against GR. The same blots were stripped and reprobed with β -actin antibody to verify equal protein loading. The results shown here are representative of three independent experiments. Image J was employed to quantify the relative expression of GR normalized to the β -actin loading control (optical density). Data are shown as the mean \pm SD (** $P < 0.001$). (C) GR was incubated with 1mM FT and NADPH for 30 min, and then GR activity was measured with GSSG addition. The results shown are representative of three independent experiments. (D) U266 cells (1×10^6 cells/well) were seeded onto 6-well plates, incubated at 37 $^{\circ}$ C with indicated concentrations of FT and Bor for 6 h. Thereafter, equal amounts of lysates were analyzed by Western blot analysis using antibodies against p-STAT3 (Tyr705), p-STAT3(Ser727), STAT3, p-STAT5(Tyr694/Tyr699), and STAT5. Image J was employed to quantify the relative expression of p-STAT3 (Tyr705), p-STAT3(Ser727), and p-STAT5(Tyr694/Tyr699) normalized to the STAT3 and STAT5 loading control (optical density). Data are

shown as the mean \pm SD (** $P < 0.001$). (E) Cells were treated with FT in the absence or presence of Bor for 24 h. The cells were stained with a Live/Dead assay reagent for 30 min and then analyzed under a fluorescence microscope as described in “Materials and methods.”

Fig. 7. Effects of FT on MM growth in xenograft mouse model. (A) Schematic representation of experimental protocol described in Materials and Methods. U266 cells (1×10^7 cells/mice) were injected subcutaneously into the right flank of the mice. The animals were randomized after 1 week of tumor cell injection into three groups based on tumor volume. Group I was given PBS (200 μ L, i.p. thrice/week), group II was given FT (20 mg/kg body weight, i.p. thrice/week), group III was given FT (40 mg/kg body weight, i.p. thrice/week). (B) Necropsy photographs of mice bearing subcutaneously implanted multiple myeloma tumors. (C) Tumor volumes in mice measured during the course of experiment and calculated using the formula $V = 4 / 3 \pi r^3$ (D) Tumor weight was measured at the end of the experiment. Columns, mean; bars, SD. (E) Body weight changes in FT treated mice.

Fig. 8. FT exerts inhibitory effects against tumor cell proliferation and angiogenesis in MM tumor tissues. (A) Immunohistochemical analysis of p-STAT3 and p-STAT5 in human multiple myeloma tumor tissues. Tumor tissues embedded in paraffin blocks were cut into 5 μ m tissue sections and probed for p-STAT3 and p-STAT5 immunoreactivity as described in the Materials and Methods section. (B) Immunohistochemical analysis of proliferation marker Ki-67 indicates the inhibition of human multiple myeloma cell proliferation in FT treated groups of animals (*upper panels*). Immunohistochemical analysis of CD31 for microvessel density in human multiple myeloma tumors indicates the inhibition of angiogenesis in FT treated groups of animals (*lower panels*). (C) Immunohistochemical analysis of GSH in human multiple myeloma tumor tissues. (D) GSH content in MM tumor tissues treated with FT for 3 weeks. Data are shown as the mean \pm SD (** $P < 0.001$). (E-G) Western blot of p-STAT3(Tyr705), p-STAT3(Ser727), STAT3, p-STAT5(Tyr694/Tyr699), STAT5, caspase-3, PARP, Bcl-2, Bcl-xL, Survivin, IAP-1, and VEGF in lysate from vehicle control, and FT treated mice. Tumor tissue lysate was prepared and Western blot analysis was performed as described in the Materials and Methods section. The same blots were stripped and reprobbed with β -actin antibody to verify equal protein loading. Image J was employed to quantify the relative expression of p-STAT3(Tyr705), p-STAT3(Ser727), STAT3, p-STAT5(Tyr694/Tyr699), STAT5, caspase-3, PARP, Bcl-2, Bcl-xL, Survivin, IAP-1, and VEGF normalized to the β -actin loading control (optical density). Data are shown as the mean \pm SD (** $P < 0.01$, *** $P < 0.001$).

8. References

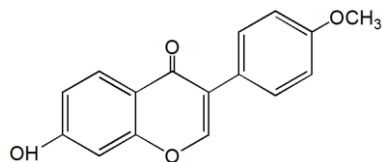
- [1] B. Sirohi, R. Powles, Multiple myeloma, *Lancet*, 363 (2004) 875-887.
- [2] R.A. Kyle, S.V. Rajkumar, Multiple myeloma, *Blood*, 111 (2008) 2962-2972.
- [3] R. Feinman, J. Koury, M. Thames, B. Barlogie, J. Epstein, D.S. Siegel, Role of NF-kappaB in the rescue of multiple myeloma cells from glucocorticoid-induced apoptosis by bcl-2, *Blood*, 93 (1999) 3044-3052.
- [4] U.K.m.f.B.C.f.S.i. Haematology, Diagnosis and management of multiple myeloma, *Br J Haematol*, 115 (2001) 522-540.
- [5] H. Brenner, A. Gonds, D. Pulte, Recent major improvement in long-term survival of younger patients with multiple myeloma, *Blood*, 111 (2008) 2521-2526.
- [6] M. Hallek, P.L. Bergsagel, K.C. Anderson, Multiple myeloma: increasing evidence for a multistep transformation process, *Blood*, 91 (1998) 3-21.
- [7] M.S. Raab, K. Podar, I. Breitkreutz, P.G. Richardson, K.C. Anderson, Multiple myeloma, *Lancet*, 374 (2009) 324-339.
- [8] A. Palumbo, K. Anderson, Multiple myeloma, *N Engl J Med*, 364 (2011) 1046-1060.
- [9] M. Chesi, P.L. Bergsagel, Many multiple myelomas: making more of the molecular mayhem, *Hematology Am Soc Hematol Educ Program*, 2011 (2011) 344-353.
- [10] A. Palumbo, S. Bringhen, H. Ludwig, M.A. Dimopoulos, J. Blade, M.V. Mateos, L. Rosinol, M. Boccadoro, M. Cavo, H. Lokhorst, S. Zweegman, E. Terpos, F. Davies, C. Driessen, P. Gimsing, M. Gramatzki, R. Hajek, H.E. Johnsen, F. Leal Da Costa, O. Sezer, A. Spencer, M. Beksac, G. Morgan, H. Einsele, J.F. San Miguel, P. Sonneveld, Personalized therapy in multiple myeloma according to patient age and vulnerability: a report of the European Myeloma Network (EMN), *Blood*, 118 (2011) 4519-4529.
- [11] M. Roussel, T. Facon, P. Moreau, J.L. Harousseau, M. Attal, Firstline treatment and maintenance in newly diagnosed multiple myeloma patients, *Recent Results Cancer Res*, 183 (2011) 189-206.
- [12] K. Suzuki, Current therapeutic strategy for multiple myeloma, *Japanese journal of clinical oncology*, 43 (2013) 116-124.
- [13] J.N. Ihle, STATs: signal transducers and activators of transcription, *Cell*, 84 (1996) 331-334.
- [14] E.Z. Chai, K.S. Siveen, M.K. Shanmugam, F. Arfuso, G. Sethi, Analysis of the intricate relationship between chronic inflammation and cancer, *Biochem J*, 468 (2015) 1-15.
- [15] E.Z. Chai, M.K. Shanmugam, F. Arfuso, A. Dharmarajan, C. Wang, A.P. Kumar, R.P. Samy, L.H. Lim, L. Wang, B.C. Goh, K.S. Ahn, K.M. Hui, G. Sethi, Targeting transcription factor STAT3 for cancer prevention and therapy, *Pharmacol Ther*, 162 (2016) 86-97.
- [16] A.L.A. Wong, J.L. Hirpara, S. Pervaiz, J.Q. Eu, G. Sethi, B.C. Goh, Do STAT3 inhibitors have potential in the future for cancer therapy?, *Expert Opin Investig Drugs*, 26 (2017) 883-887.
- [17] M. Furqan, N. Mukhi, B. Lee, D. Liu, Dysregulation of JAK-STAT pathway in hematological malignancies and JAK inhibitors for clinical application, *Biomark Res*, 1 (2013) 5.
- [18] J.E. Darnell, Jr., Transcription factors as targets for cancer therapy, *Nature reviews. Cancer*, 2 (2002) 740-749.
- [19] S. Li, S.J. Priceman, H. Xin, W. Zhang, J. Deng, Y. Liu, J. Huang, W. Zhu, M. Chen, W. Hu, X. Deng, J. Zhang, H. Yu, G. He, Icaritin inhibits JAK/STAT3 signaling and growth of renal cell carcinoma, *PLoS One*, 8 (2013) e81657.
- [20] A. Subramaniam, M.K. Shanmugam, T.H. Ong, F. Li, E. Perumal, L. Chen, S. Vali, T. Abbasi, S. Kapoor, K.S. Ahn, A.P. Kumar, K.M. Hui, G. Sethi, Emodin inhibits growth and induces apoptosis in an orthotopic hepatocellular carcinoma model by blocking activation of STAT3, *Br J Pharmacol*, 170 (2013) 807-821.
- [21] C. Kim, S.K. Cho, S. Kapoor, A. Kumar, S. Vali, T. Abbasi, S.H. Kim, G. Sethi, K.S. Ahn, beta-Caryophyllene oxide inhibits constitutive and inducible STAT3 signaling pathway through induction of the SHP-1 protein tyrosine phosphatase, *Mol Carcinog*, 53 (2014) 793-806.
- [22] S.M. Kim, C. Kim, H. Bae, J.H. Lee, S.H. Baek, D. Nam, W.S. Chung, B.S. Shim, S.G. Lee, S.H. Kim, G. Sethi, K.S. Ahn, 6-Shogaol exerts anti-proliferative and pro-apoptotic effects through the modulation of STAT3 and MAPKs signaling pathways, *Mol Carcinog*, 54 (2015) 1132-1146.
- [23] J.H. Lee, C. Kim, S.H. Kim, G. Sethi, K.S. Ahn, Farnesol inhibits tumor growth and enhances the anticancer effects of bortezomib in multiple myeloma xenograft mouse model through the modulation of STAT3 signaling pathway, *Cancer Lett*, 360 (2015) 280-293.
- [24] J.H. Lee, C. Kim, S.H. Baek, J.H. Ko, S.G. Lee, W.M. Yang, J.Y. Um, G. Sethi, K.S. Ahn, Capsazepine inhibits JAK/STAT3 signaling, tumor growth, and cell survival in prostate cancer, *Oncotarget*, 8 (2017) 17700-17711.
- [25] R. Buettner, L.B. Mora, R. Jove, Activated STAT signaling in human tumors provides novel molecular targets for therapeutic intervention, *Clinical cancer research : an official journal of the American Association for Cancer Research*, 8 (2002) 945-954.
- [26] A.M. Weaver, C.M. Silva, Signal transducer and activator of transcription 5b: a new target of breast tumor kinase/protein tyrosine kinase 6, *Breast Cancer Res*, 9 (2007) R79.
- [27] H. Wang, F. Lafdil, X. Kong, B. Gao, Signal transducer and activator of transcription 3 in liver diseases: a novel therapeutic target, *Int J Biol Sci*, 7 (2011) 536-550.
- [28] J.H. Lee, C. Kim, G. Sethi, K.S. Ahn, Brassinin inhibits STAT3 signaling pathway through modulation of PIAS-3 and SOCS-3 expression and sensitizes human lung cancer xenograft in nude mice to paclitaxel, *Oncotarget*, 6 (2015) 6386-6405.
- [29] X. Dai, K.S. Ahn, C. Kim, K.S. Siveen, T.H. Ong, M.K. Shanmugam, F. Li, J. Shi, A.P. Kumar, L.Z. Wang, B.C. Goh, J. Magae, K.M. Hui, G. Sethi, Ascochlorin, an isoprenoid antibiotic inhibits growth and invasion of hepatocellular carcinoma by targeting STAT3 signaling cascade through the induction of PIAS3, *Mol Oncol*, 9 (2015) 818-833.

- [30] S.H. Baek, J.H. Lee, C. Kim, J.H. Ko, S.H. Ryu, S.G. Lee, W.M. Yang, J.Y. Um, A. Chinnathambi, S.A. Alharbi, G. Sethi, K.S. Ahn, Ginkgolic Acid C 17:1, Derived from Ginkgo biloba Leaves, Suppresses Constitutive and Inducible STAT3 Activation through Induction of PTEN and SHP-1 Tyrosine Phosphatase, *Molecules*, 22 (2017).
- [31] Z. Ren, T.S. Schaefer, ErbB-2 activates Stat3 alpha in a Src- and JAK2-dependent manner, *The Journal of biological chemistry*, 277 (2002) 38486-38493.
- [32] M.K. Shanmugam, P. Rajendran, F. Li, C. Kim, S. Sikka, K.S. Siveen, A.P. Kumar, K.S. Ahn, G. Sethi, Abrogation of STAT3 signaling cascade by zerumbone inhibits proliferation and induces apoptosis in renal cell carcinoma xenograft mouse model, *Mol Carcinog*, (2014).
- [33] K.S. Siveen, S. Sikka, R. Surana, X. Dai, J. Zhang, A.P. Kumar, B.K. Tan, G. Sethi, A. Bishayee, Targeting the STAT3 signaling pathway in cancer: role of synthetic and natural inhibitors, *Biochim Biophys Acta*, 1845 (2014) 136-154.
- [34] J. Zhang, S. Sikka, K.S. Siveen, J.H. Lee, J.Y. Um, A.P. Kumar, A. Chinnathambi, S.A. Alharbi, Basappa, K.S. Rangappa, G. Sethi, K.S. Ahn, Cardamonin represses proliferation, invasion, and causes apoptosis through the modulation of signal transducer and activator of transcription 3 pathway in prostate cancer, *Apoptosis*, 22 (2017) 158-168.
- [35] A.C. Bharti, N. Donato, B.B. Aggarwal, Curcumin (diferuloylmethane) inhibits constitutive and IL-6-inducible STAT3 phosphorylation in human multiple myeloma cells, *J Immunol*, 171 (2003) 3863-3871.
- [36] S. Xi, Q. Zhang, W.E. Gooding, T.E. Smithgall, J.R. Grandis, Constitutive activation of Stat5b contributes to carcinogenesis in vivo, *Cancer Res*, 63 (2003) 6763-6771.
- [37] F. Li, P. Rajendran, G. Sethi, Thymoquinone inhibits proliferation, induces apoptosis and chemosensitizes human multiple myeloma cells through suppression of signal transducer and activator of transcription 3 activation pathway, *Br J Pharmacol*, 161 (2010) 541-554.
- [38] R. Kannaiyan, H.S. Hay, P. Rajendran, F. Li, M.K. Shanmugam, S. Vali, T. Abbasi, S. Kapoor, A. Sharma, A.P. Kumar, W.J. Chng, G. Sethi, Celastrol inhibits proliferation and induces chemosensitization through down-regulation of NF-kappaB and STAT3 regulated gene products in multiple myeloma cells, *Br J Pharmacol*, 164 (2011) 1506-1521.
- [39] H. Yu, R. Jove, The STATs of cancer--new molecular targets come of age, *Nature reviews. Cancer*, 4 (2004) 97-105.
- [40] D.J. Newman, Natural products as leads to potential drugs: an old process or the new hope for drug discovery?, *J Med Chem*, 51 (2008) 2589-2599.
- [41] M.K. Shanmugam, R. Kannaiyan, G. Sethi, Targeting cell signaling and apoptotic pathways by dietary agents: role in the prevention and treatment of cancer, *Nutr Cancer*, 63 (2011) 161-173.
- [42] C.H. Tang, G. Sethi, P.L. Kuo, Novel medicines and strategies in cancer treatment and prevention, *Biomed Res Int*, 2014 (2014) 474078.
- [43] Y.S. Hsieh, S.F. Yang, G. Sethi, D.N. Hu, Natural bioactives in cancer treatment and prevention, *Biomed Res Int*, 2015 (2015) 182835.
- [44] A. Bishayee, G. Sethi, Bioactive natural products in cancer prevention and therapy: Progress and promise, *Semin Cancer Biol*, 40-41 (2016) 1-3.
- [45] M.K. Shanmugam, J.H. Lee, E.Z. Chai, M.M. Kanchi, S. Kar, F. Arfuso, A. Dharmarajan, A.P. Kumar, P.S. Ramar, C.Y. Looi, M.R. Mustafa, V. Tergaonkar, A. Bishayee, K.S. Ahn, G. Sethi, Cancer prevention and therapy through the modulation of transcription factors by bioactive natural compounds, *Semin Cancer Biol*, (2016).
- [46] R. Zhou, L. Xu, M. Ye, M. Liao, H. Du, H. Chen, Formononetin inhibits migration and invasion of MDA-MB-231 and 4T1 breast cancer cells by suppressing MMP-2 and MMP-9 through PI3K/AKT signaling pathways, *Horm Metab Res*, 46 (2014) 753-760.
- [47] Y. Wu, X. Zhang, Z. Li, H. Yan, J. Qin, T. Li, Formononetin inhibits human bladder cancer cell proliferation and invasiveness via regulation of miR-21 and PTEN, *Food Funct*, 8 (2017) 1061-1066.
- [48] X.Y. Wu, H. Xu, Z.F. Wu, C. Chen, J.Y. Liu, G.N. Wu, X.Q. Yao, F.K. Liu, G. Li, L. Shen, Formononetin, a novel FGFR2 inhibitor, potently inhibits angiogenesis and tumor growth in preclinical models, *Oncotarget*, 6 (2015) 44563-44578.
- [49] J. Chen, J. Zeng, M. Xin, W. Huang, X. Chen, Formononetin induces cell cycle arrest of human breast cancer cells via IGF1/PI3K/Akt pathways in vitro and in vivo, *Horm Metab Res*, 43 (2011) 681-686.
- [50] Y.M. Jin, T.M. Xu, Y.H. Zhao, Y.C. Wang, M.H. Cui, In vitro and in vivo anti-cancer activity of formononetin on human cervical cancer cell line HeLa, *Tumour Biol*, 35 (2014) 2279-2284.
- [51] T. Li, X. Zhao, Z. Mo, W. Huang, H. Yan, Z. Ling, Y. Ye, Formononetin promotes cell cycle arrest via downregulation of Akt/Cyclin D1/CDK4 in human prostate cancer cells, *Cell Physiol Biochem*, 34 (2014) 1351-1358.
- [52] Y. Yang, Y. Zhao, X. Ai, B. Cheng, S. Lu, Formononetin suppresses the proliferation of human non-small cell lung cancer through induction of cell cycle arrest and apoptosis, *Int J Clin Exp Pathol*, 7 (2014) 8453-8461.
- [53] J. Huang, M. Xie, P. Gao, Y. Ye, Y. Liu, Y. Zhao, W. Luo, Z. Ling, Y. Cao, S. Zhang, F. Gao, W. Tang, Antiproliferative effects of formononetin on human colorectal cancer via suppressing cell growth in vitro and in vivo, *Process Biochemistry*, 50 (2015) 912-917.
- [54] C. Qi, M. Xie, J. Liang, H. Li, Z. Li, S. Shi, X. Yang, Z. Wang, J. Tang, A. Tang, Formononetin targets the MAPK and PI3K/Akt pathways to induce apoptosis in human nasopharyngeal carcinoma cells in vitro and in vivo. *Int J Clin Exp Med*, 9(2016):1180-1189.
- [55] D. Sun, Y. Lu, S.J. Zhang, K.G. Wang, Z. Sun, Research on the effect of formononetin on photodynamic therapy in K562 cells, *Gen Physiol Biophys*, 36 (2017) 423-430.
- [56] K.K. Auyeung, P.C. Law, J.K. Ko, Novel anti-angiogenic effects of formononetin in human colon cancer cells and tumor

xenograft, *Oncology reports*, 28 (2012) 2188-2194.

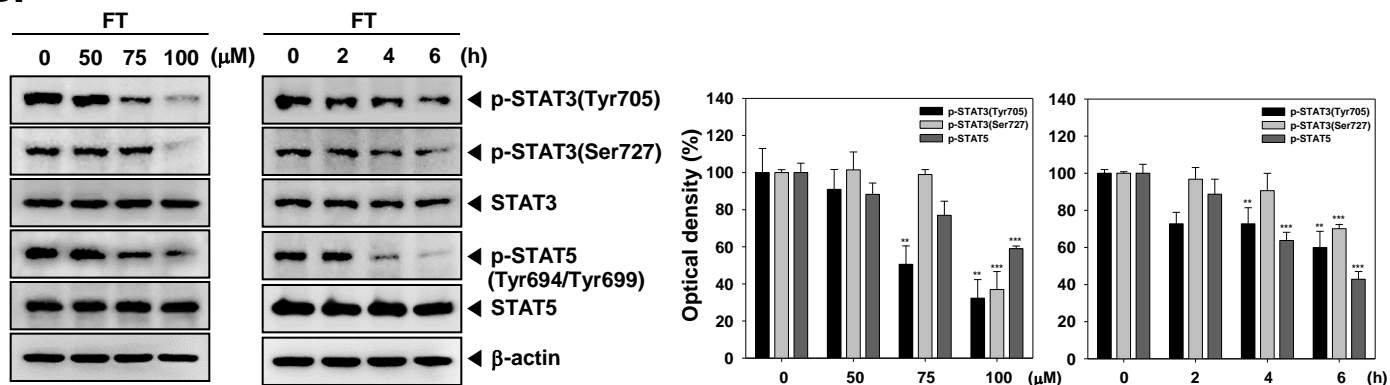
- [57] Y.H. Guo, Y. Wang, M. Xin, Low concentration of formononetin stimulates the proliferation of nasopharyngeal carcinoma cell line CNE2 by upregulating bcl-2 and p-ERK1/2 expression, *Pharm Biol*, (2016) 1-6.
- [58] S. Li, Y. Dang, X. Zhou, B. Huang, X. Huang, Z. Zhang, Y.W. Kwan, S.W. Chan, G.P. Leung, S.M. Lee, M.P. Hoi, Formononetin promotes angiogenesis through the estrogen receptor alpha-enhanced ROCK pathway, *Sci Rep*, 5 (2015) 16815.
- [59] A. Beldi-Ferchiou, N. Skouri, C. Ben Ali, I. Safra, A. Abdelkefi, S. Ladeb, K. Mrad, T. Ben Othman, M. Ben Ahmed, Abnormal repression of SHP-1, SHP-2 and SOCS-1 transcription sustains the activation of the JAK/STAT3 pathway and the progression of the disease in multiple myeloma, *PLoS One*, 12 (2017) e0174835.
- [60] P. Rajendran, F. Li, M.K. Shanmugam, R. Kannaiyan, J.N. Goh, K.F. Wong, W. Wang, E. Khin, V. Tergaonkar, A.P. Kumar, J.M. Luk, G. Sethi, Celastrol suppresses growth and induces apoptosis of human hepatocellular carcinoma through the modulation of STAT3/JAK2 signaling cascade in vitro and in vivo, *Cancer Prev Res (Phila)*, 5 (2012) 631-643.
- [61] A. Subramaniam, M.K. Shanmugam, E. Perumal, F. Li, A. Nachiyappan, X. Dai, S.N. Swamy, K.S. Ahn, A.P. Kumar, B.K. Tan, K.M. Hui, G. Sethi, Potential role of signal transducer and activator of transcription (STAT)3 signaling pathway in inflammation, survival, proliferation and invasion of hepatocellular carcinoma, *Biochim Biophys Acta*, 1835 (2013) 46-60.
- [62] C.L. Yu, D.J. Meyer, G.S. Campbell, A.C. Lerner, C. Carter-Su, J. Schwartz, R. Jove, Enhanced DNA-binding activity of a Stat3-related protein in cells transformed by the Src oncoprotein, *Science*, 269 (1995) 81-83.
- [63] S.J. Schreiner, A.P. Schiavone, T.E. Smithgall, Activation of STAT3 by the Src family kinase Hck requires a functional SH3 domain, *The Journal of biological chemistry*, 277 (2002) 45680-45687.
- [64] J.P. Alao, The regulation of cyclin D1 degradation: roles in cancer development and the potential for therapeutic invention, *Mol Cancer*, 6 (2007) 24.
- [65] Y.H. Choi, L. Zhang, W.H. Lee, K.Y. Park, Genistein-induced G2/M arrest is associated with the inhibition of cyclin B1 and the induction of p21 in human breast carcinoma cells, *Int J Oncol*, 13 (1998) 391-396.
- [66] M.L. Circu, T.Y. Aw, Glutathione and apoptosis, *Free Radic Res*, 42 (2008) 689-706.
- [67] B. Peng, L. Xu, F. Cao, T. Wei, C. Yang, G. Uzan, D. Zhang, HSP90 inhibitor, celastrol, arrests human monocytic leukemia cell U937 at G0/G1 in thiol-containing agents reversible way, *Mol Cancer*, 9 (2010) 79.
- [68] S. Krifka, K.A. Hiller, G. Spagnuolo, A. Jewett, G. Schmalz, H. Schweikl, The influence of glutathione on redox regulation by antioxidant proteins and apoptosis in macrophages exposed to 2-hydroxyethyl methacrylate (HEMA), *Biomaterials*, 33 (2012) 5177-5186.
- [69] L. Flohe, The fairytale of the GSSG/GSH redox potential, *Biochim Biophys Acta*, 1830 (2013) 3139-3142.
- [70] M. Deponte, Glutathione catalysis and the reaction mechanisms of glutathione-dependent enzymes, *Biochim Biophys Acta*, 1830 (2013) 3217-3266.
- [71] T. Toyonaga, K. Nakano, M. Nagano, G. Zhao, K. Yamaguchi, S. Kuroki, T. Eguchi, K. Chijiwa, M. Tsuneyoshi, M. Tanaka, Blockade of constitutively activated Janus kinase/signal transducer and activator of transcription-3 pathway inhibits growth of human pancreatic cancer, *Cancer Lett*, 201 (2003) 107-116.
- [72] P. Yue, J. Turkson, Targeting STAT3 in cancer: how successful are we?, *Expert Opin Investig Drugs*, 18 (2009) 45-56.
- [73] R. Catlett-Falcone, T.H. Landowski, M.M. Oshiro, J. Turkson, A. Levitzki, R. Savino, G. Ciliberto, L. Moscinski, J.L. Fernandez-Luna, G. Nunez, W.S. Dalton, R. Jove, Constitutive activation of Stat3 signaling confers resistance to apoptosis in human U266 myeloma cells, *Immunity*, 10 (1999) 105-115.
- [74] C. Li, Z. Yang, C. Zhai, W. Qiu, D. Li, Z. Yi, L. Wang, J. Tang, M. Qian, J. Luo, M. Liu, Maslinic acid potentiates the anti-tumor activity of tumor necrosis factor alpha by inhibiting NF-kappaB signaling pathway, *Mol Cancer*, 9 (2010) 73.
- [75] M. Nielsen, C.G. Kaestel, K.W. Eriksen, A. Woetmann, T. Stokkedal, K. Kaltoft, C. Geisler, C. Ropke, N. Odum, Inhibition of constitutively activated Stat3 correlates with altered Bcl-2/Bax expression and induction of apoptosis in mycosis fungoides tumor cells, *Leukemia*, 13 (1999) 735-738.
- [76] N.N. Danial, A. Pernis, P.B. Rothman, Jak-STAT signaling induced by the v-abl oncogene, *Science*, 269 (1995) 1875-1877.
- [77] P.L. Simonian, D.A. Grillot, G. Nunez, Bcl-2 and Bcl-XL can differentially block chemotherapy-induced cell death, *Blood*, 90 (1997) 1208-1216.
- [78] W. Hu, Z. Xiao, Formononetin induces apoptosis of human osteosarcoma cell line U2OS by regulating the expression of Bcl-2, Bax and MiR-375 in vitro and in vivo, *Cell Physiol Biochem*, 37 (2015) 933-939.
- [79] P.S. Hole, R.L. Darley, A. Tonks, Do reactive oxygen species play a role in myeloid leukemias?, *Blood*, 117 (2011) 5816-5826.
- [80] M.A. Ogasawara, H. Zhang, Redox regulation and its emerging roles in stem cells and stem-like cancer cells, *Antioxid Redox Signal*, 11 (2009) 1107-1122.
- [81] S.W. Ryter, H.P. Kim, A. Hoetzel, J.W. Park, K. Nakahira, X. Wang, A.M. Choi, Mechanisms of cell death in oxidative stress, *Antioxid Redox Signal*, 9 (2007) 49-89.

A.

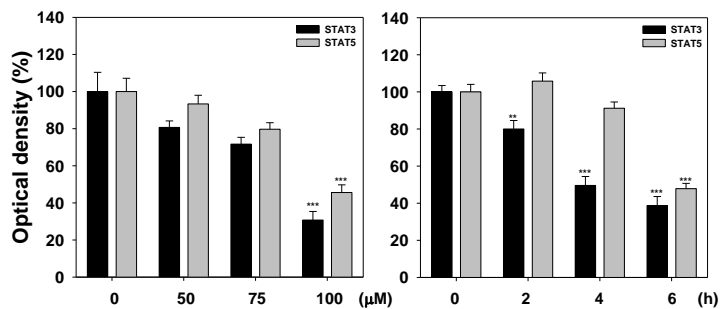
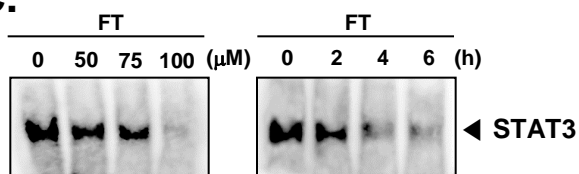


Formononetin (FT)
7-hydroxy-3-(4-methoxyphenyl)chromen-4-one
[MW : 268]

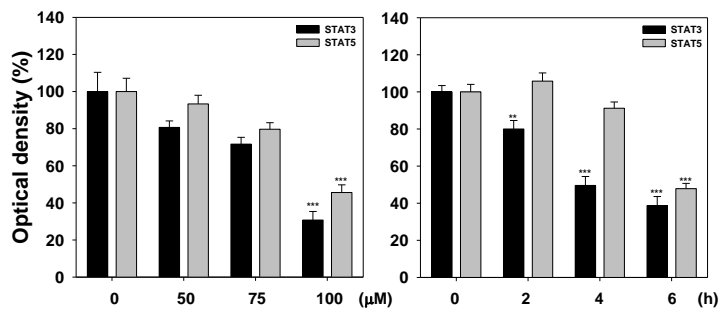
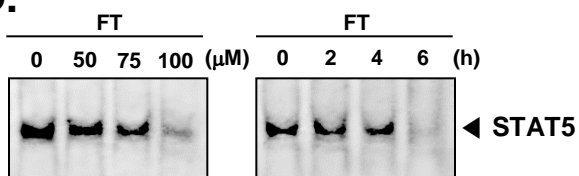
B.



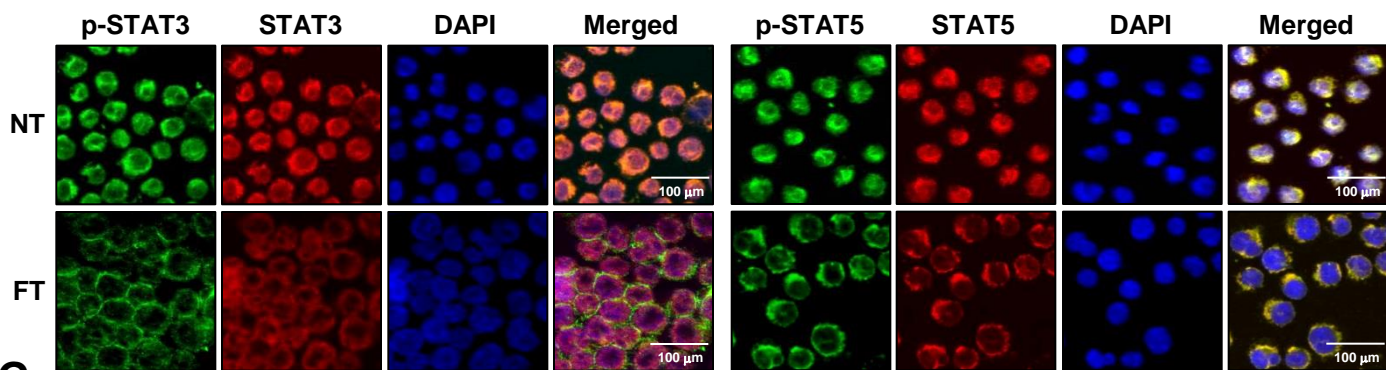
C.



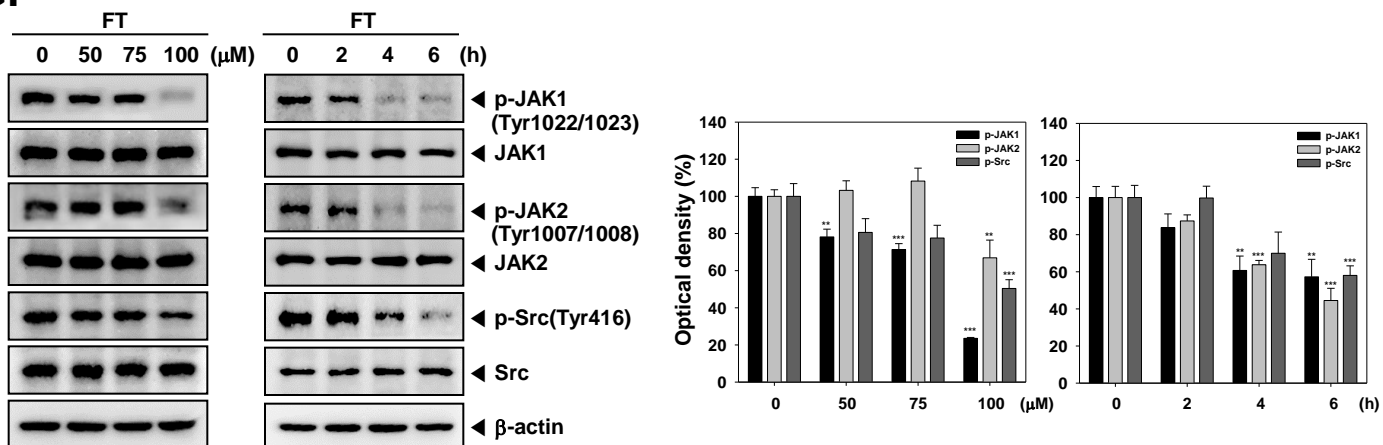
D.



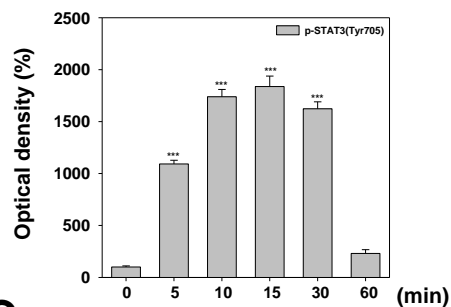
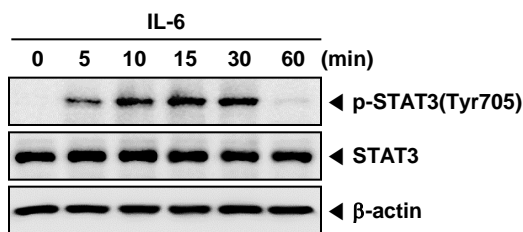
E.



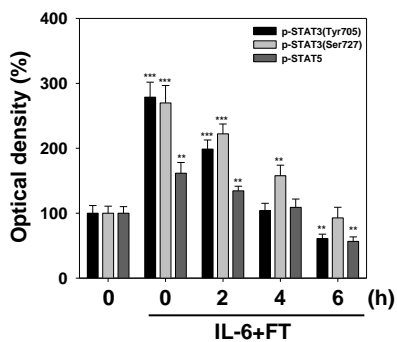
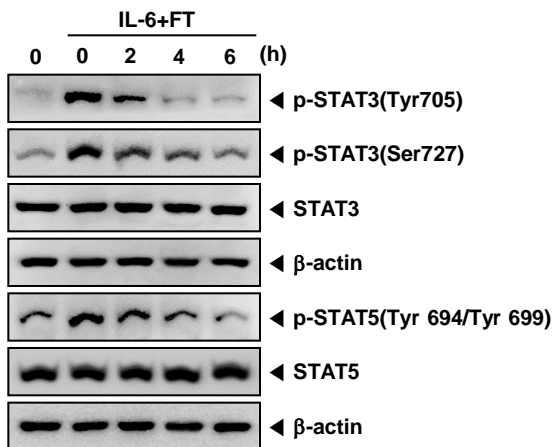
G.



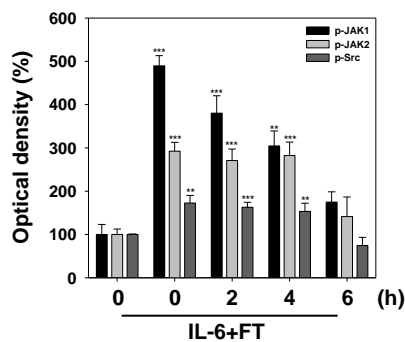
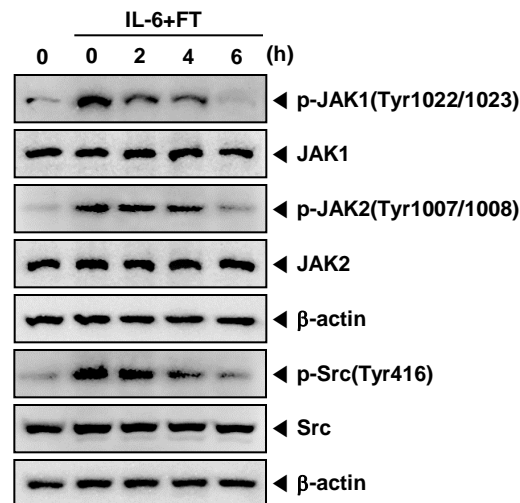
A.



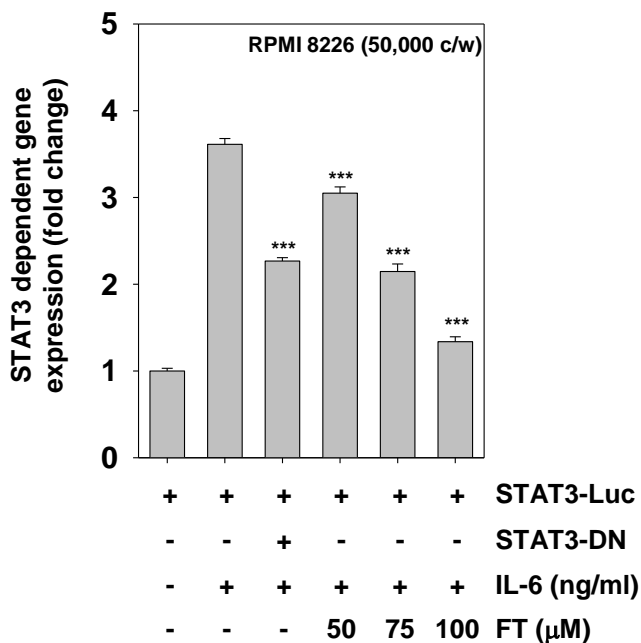
B.



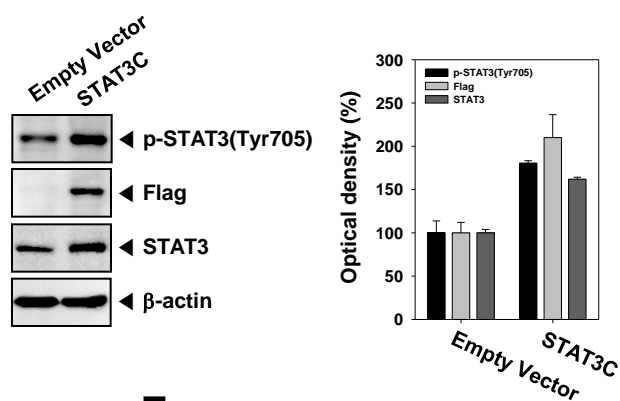
C.



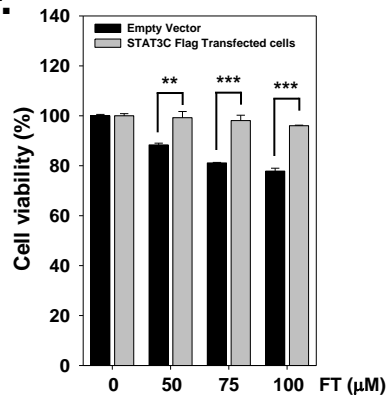
D.

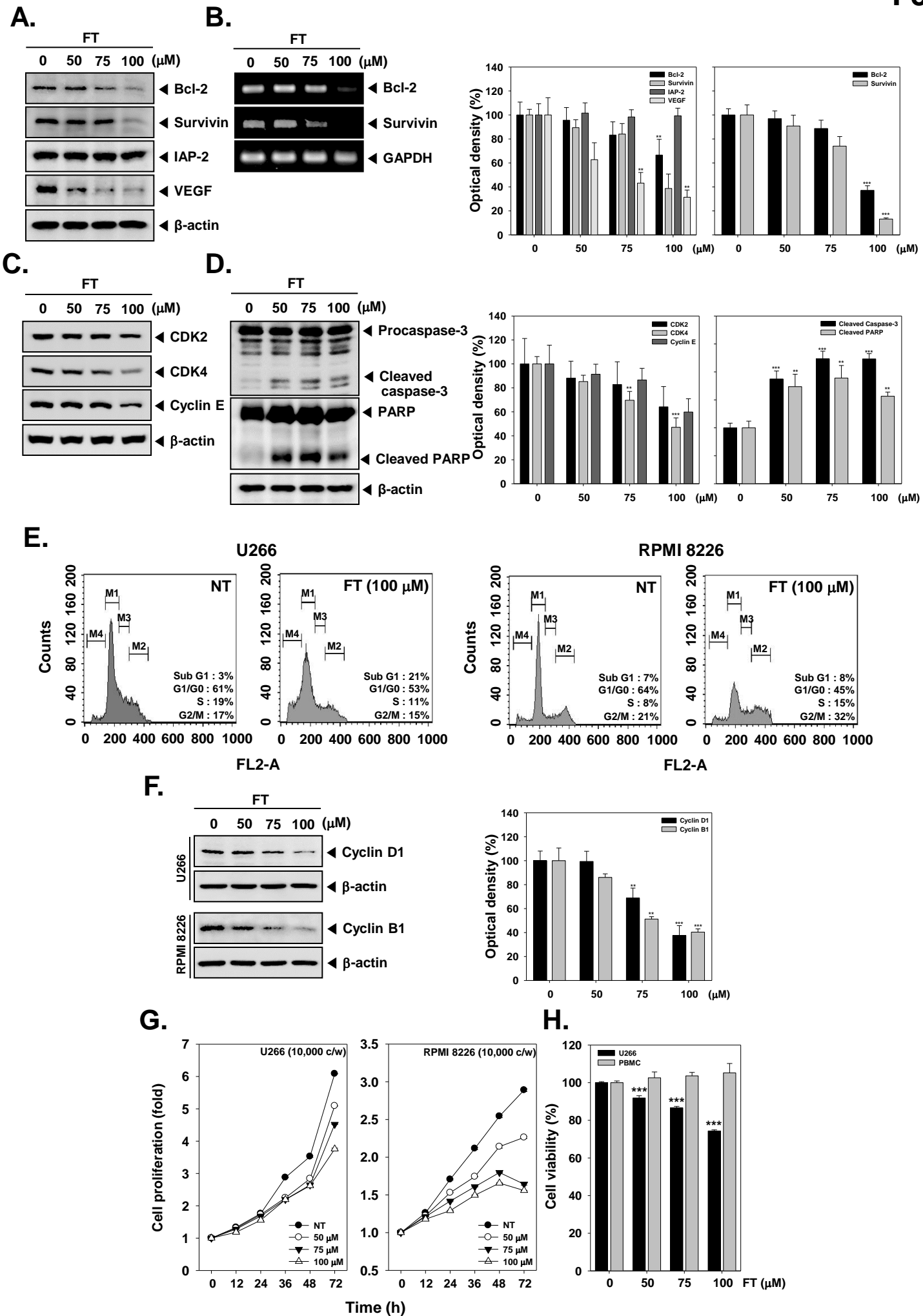


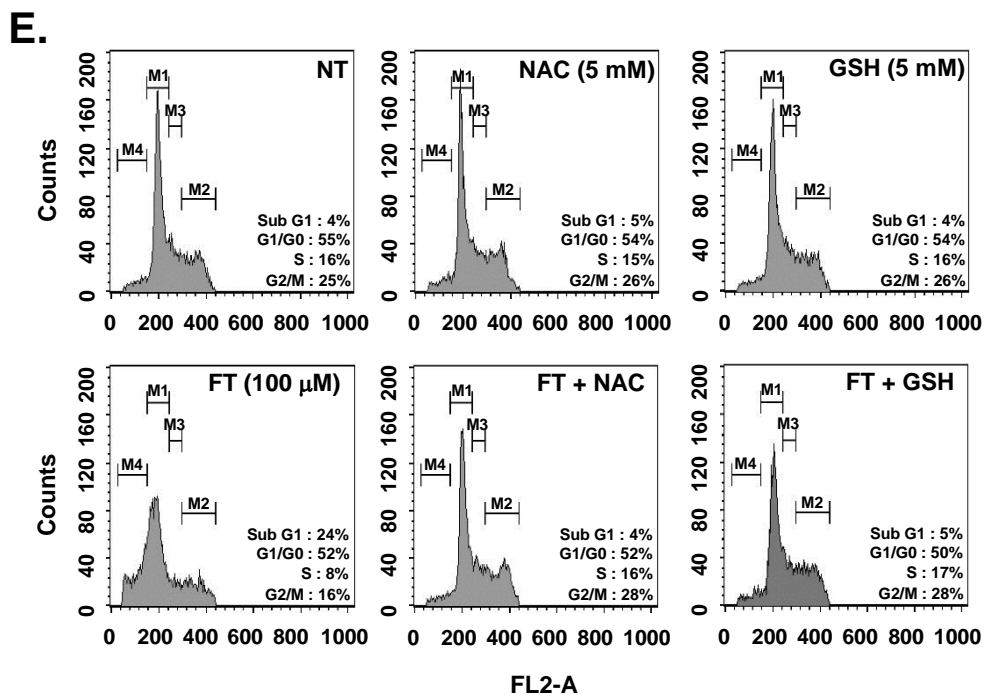
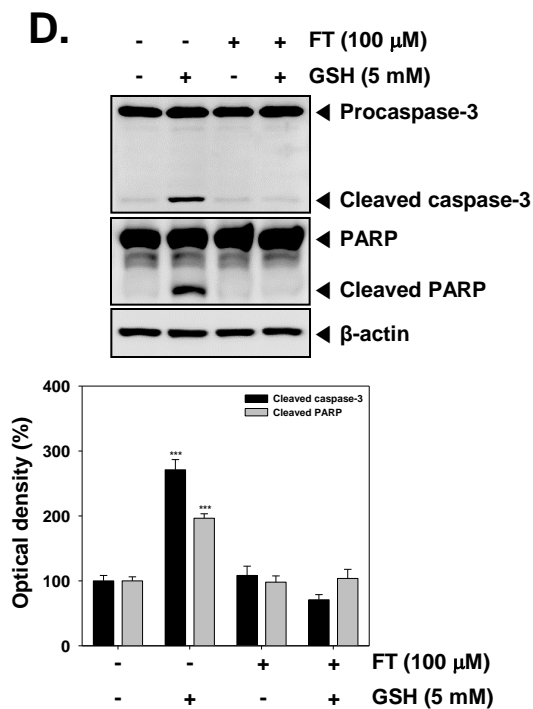
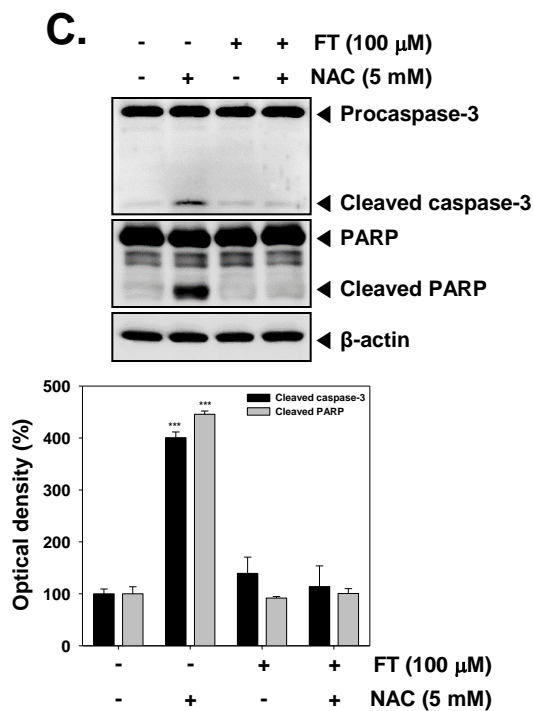
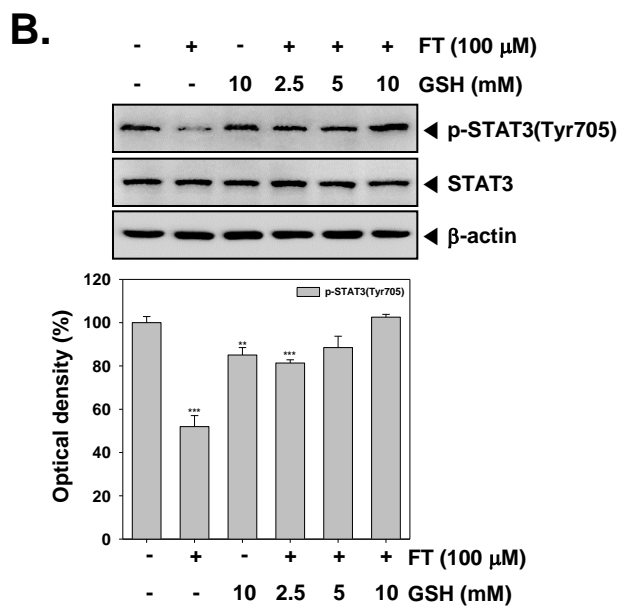
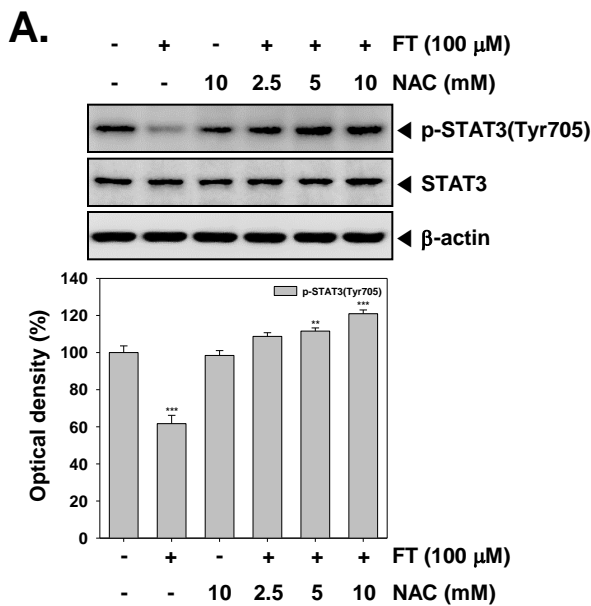
E.

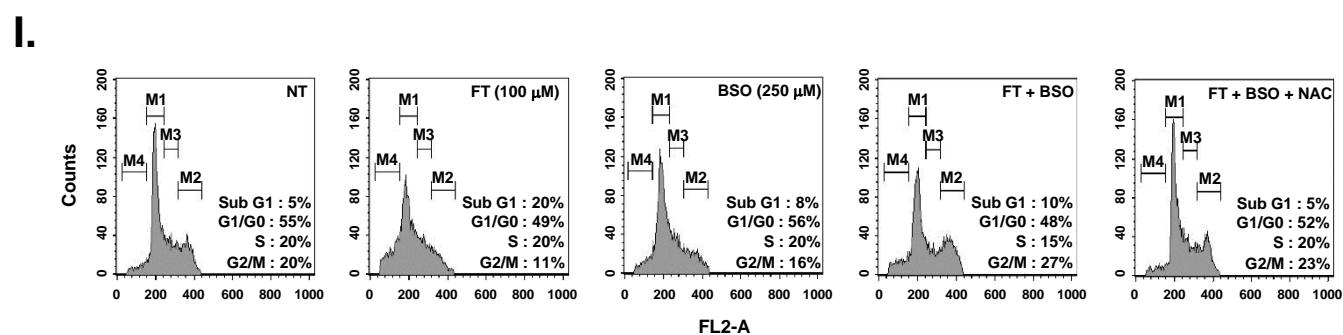
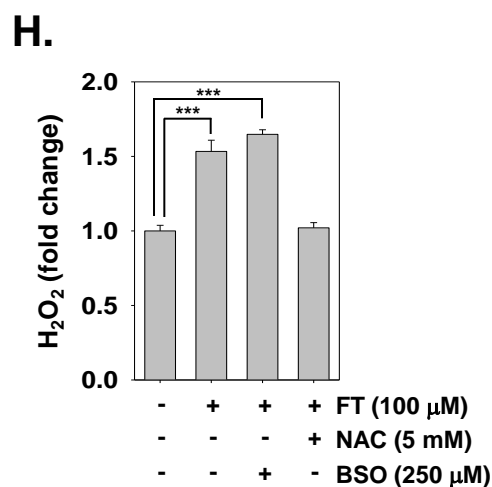
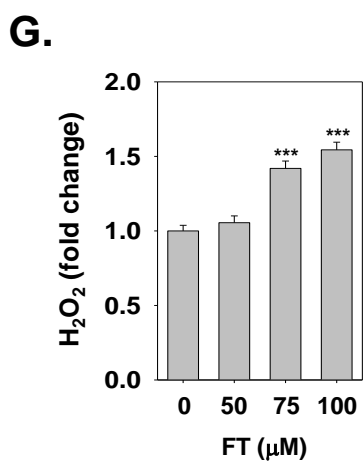
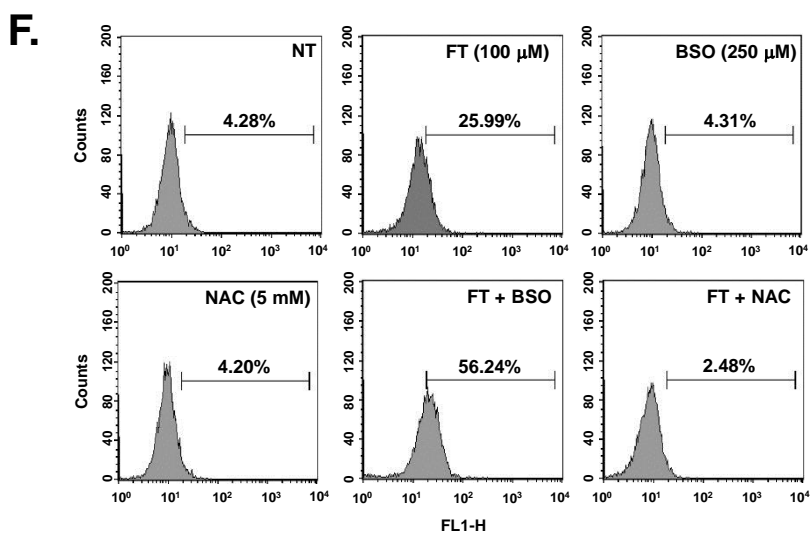
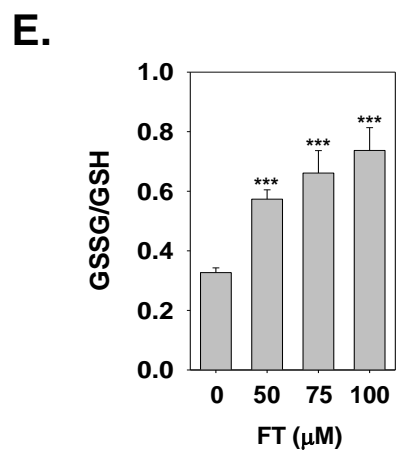
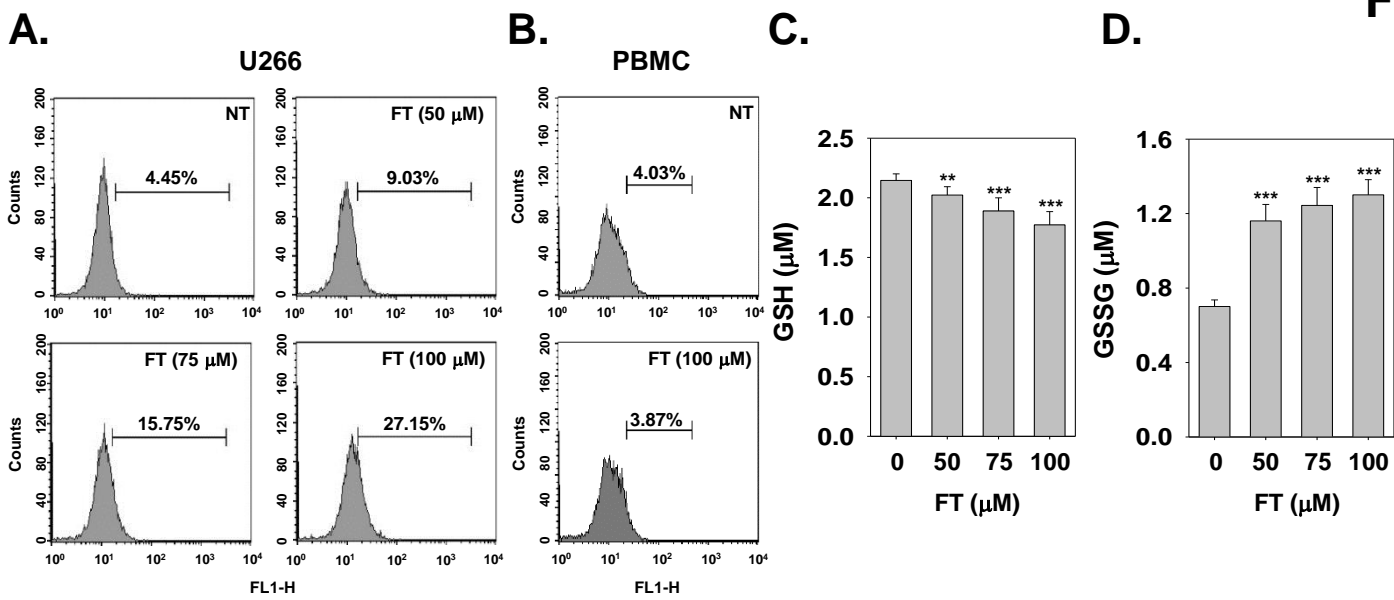


F.

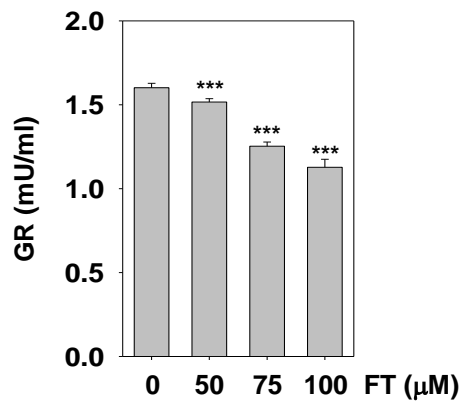




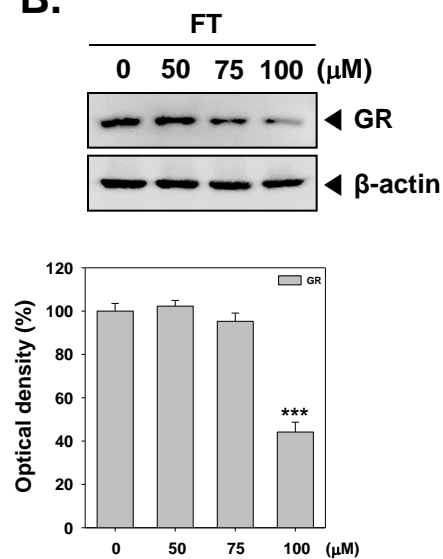




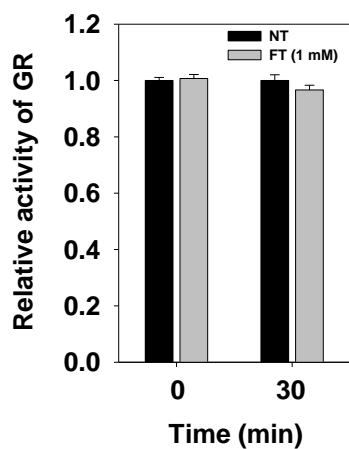
A.



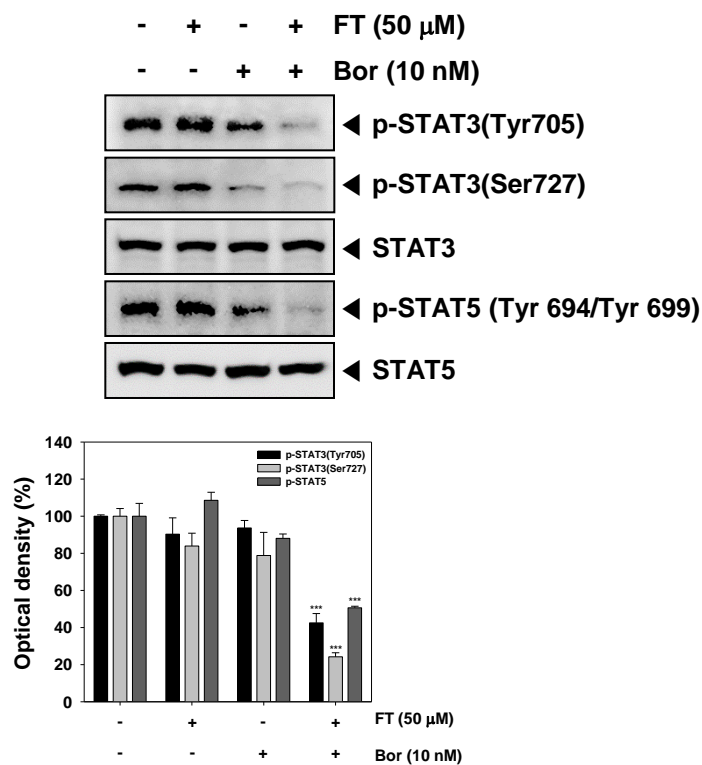
B.



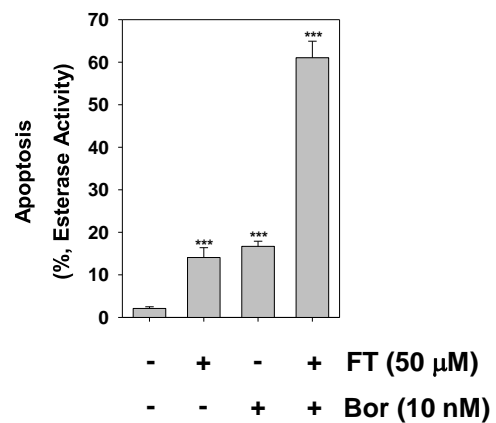
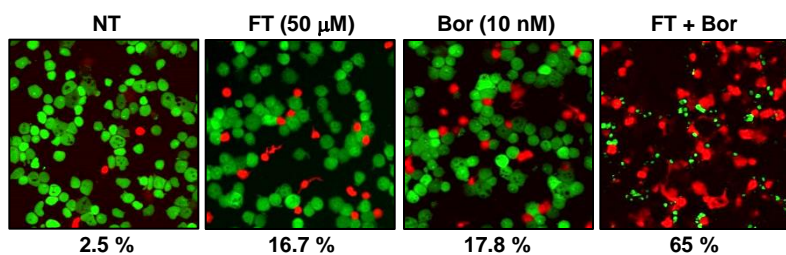
C.



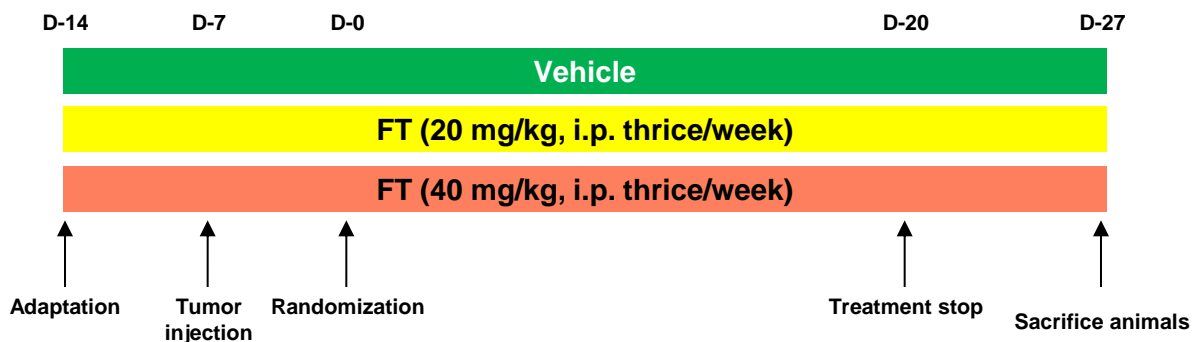
D.



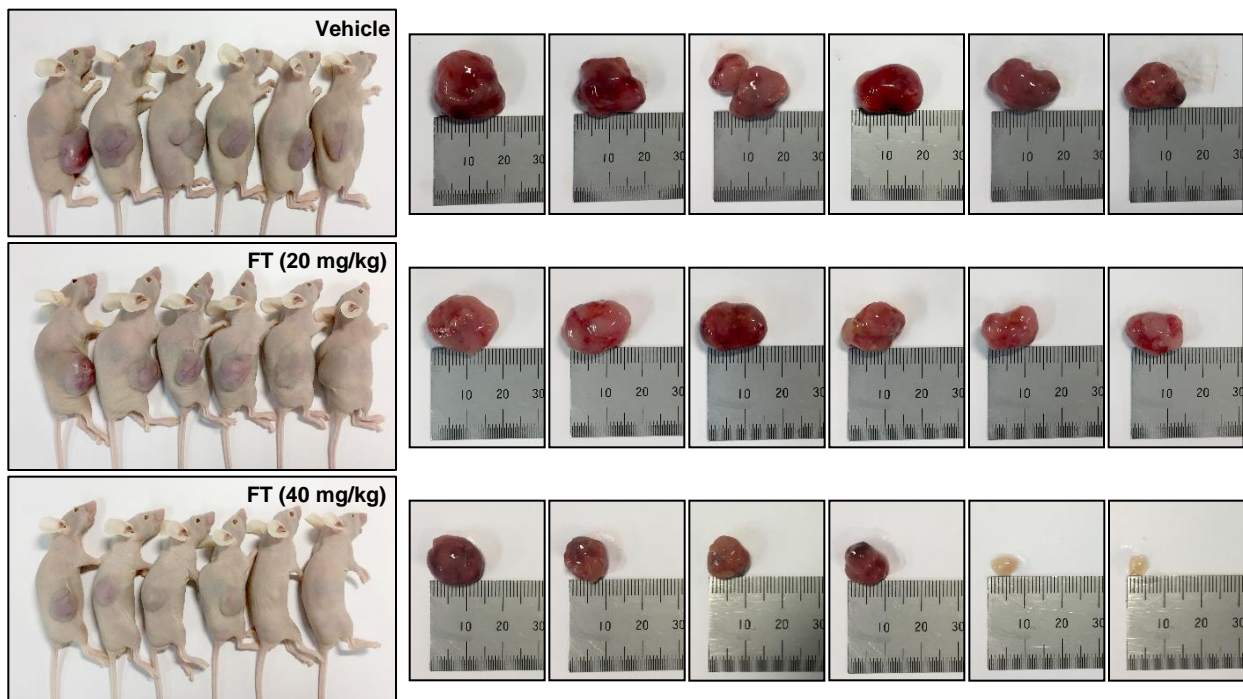
E.



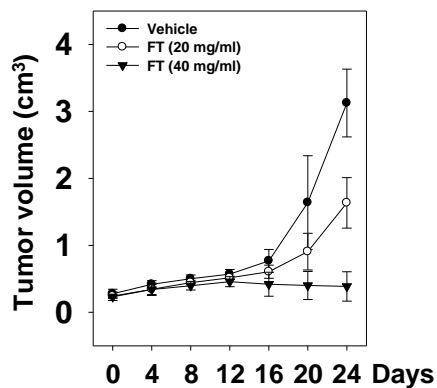
A.



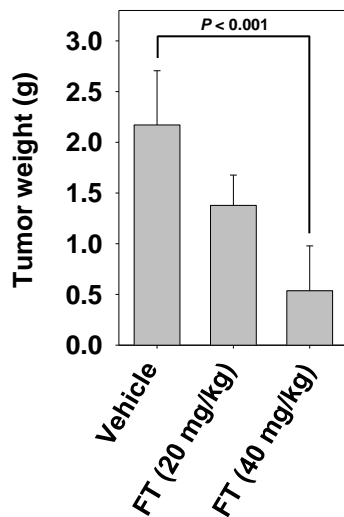
B.



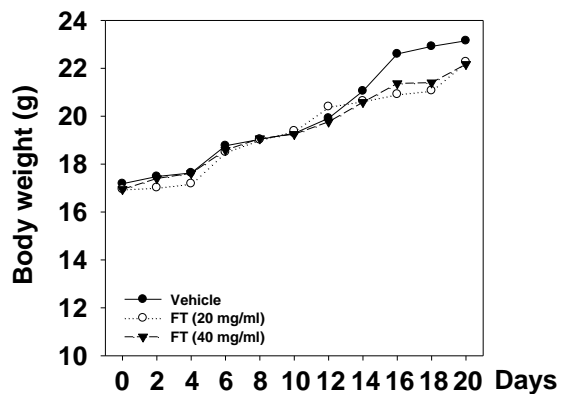
C.

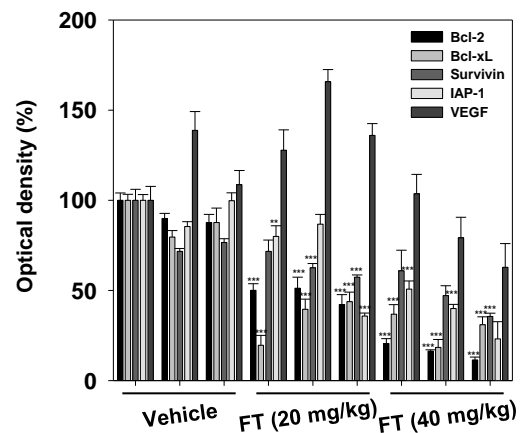
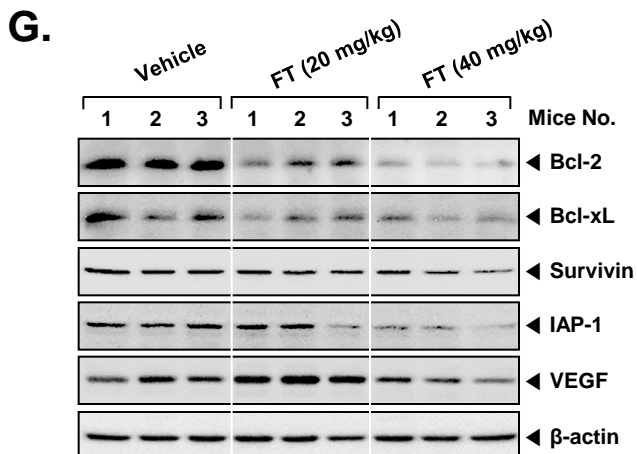
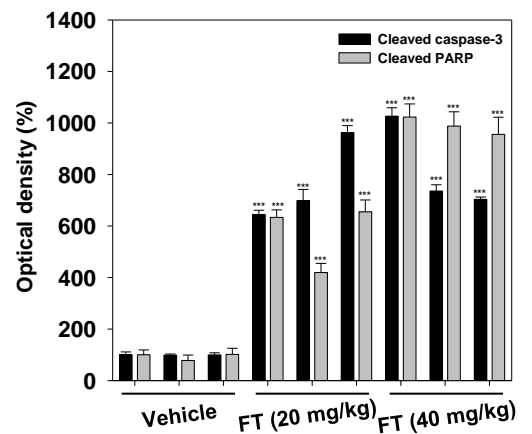
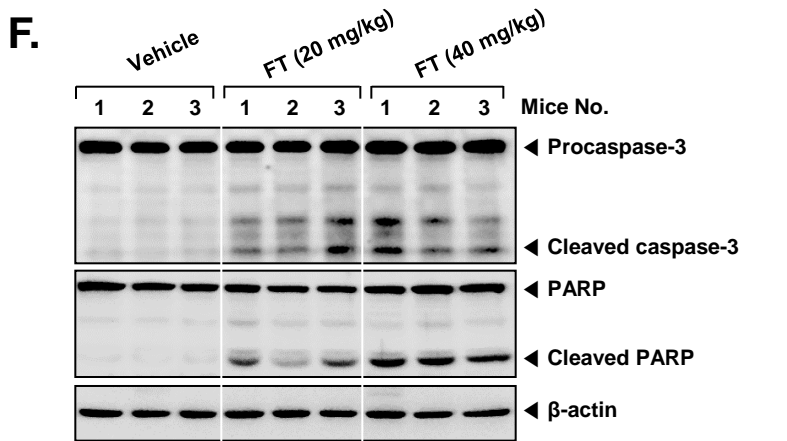
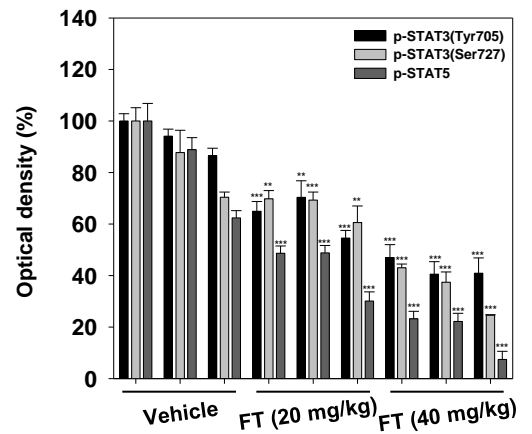
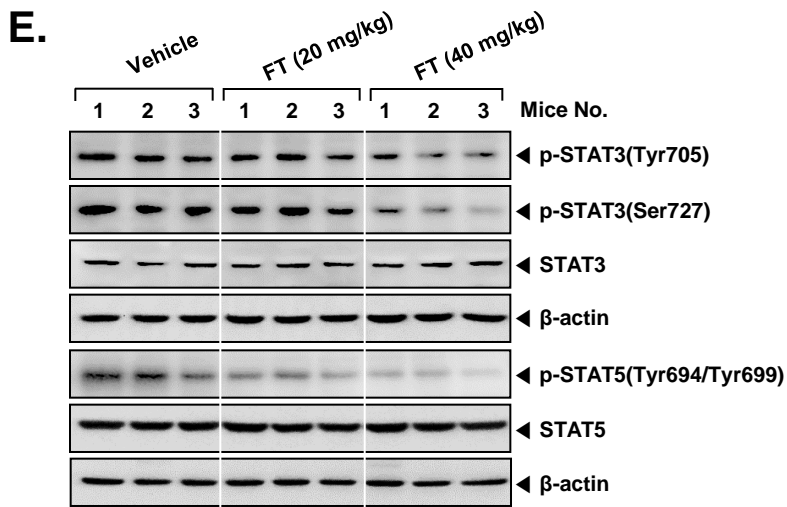
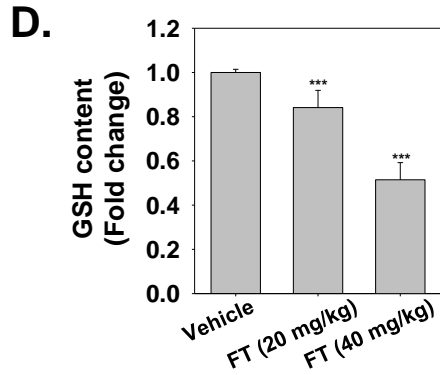
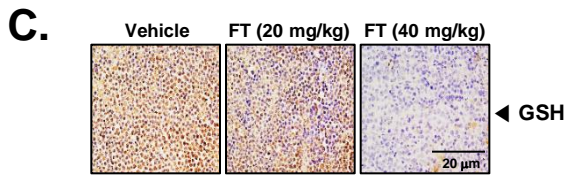
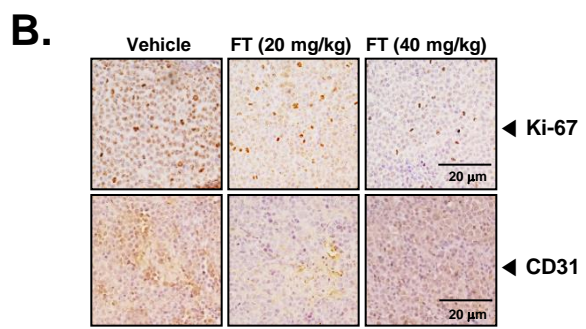
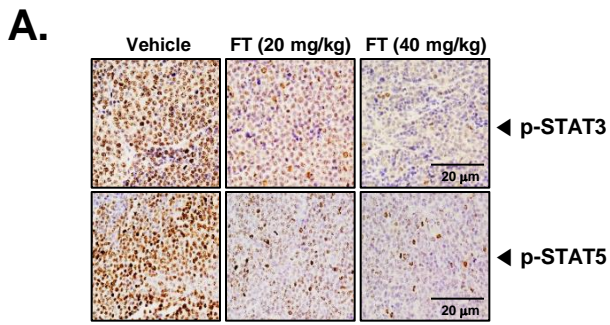


D.



E.





HIGHLIGHTS

- Formononetin (FT) attenuated constitutive STAT3 and STAT5 activation in MM cells *via* an increased production of reactive oxygen species (ROS) due to GSH/GSSG imbalance.
- FT significantly attenuated the tumor growth in the multiple myeloma xenograft mouse model without exhibiting any significant adverse effects.
- FT also downregulated the expression of STAT3 regulated gene products in tumor tissues obtained from xenograft mouse model.